Precipitation in the mountains of Central Asia: isotopic composition and source regions

Zarina Saidaliyeva[1], Maria Shahgedanova[1], Vadim Yapiyev[1,2], Andrew John Wade[1], Fakhriddin Akbarov[3], Mukhammed Esenaman uulu[4], Olga Kalashnikova[4], Vassiliy Kapitsa[5], Nikolay Kasatkin [5], Ilkhomiddin Rakhimov[6], Rysbek Satylkanov[7], Daniiar Sayakbaev[7], Eleonora Semakova[8], Igor Severskiy[5], Maxim Petrov[3], Gulomjon Umirzakov[9,10], and Ryskul Usubaliev[4]

[1]Department of Geography and Environmental Science, University of Reading, Reading, RG66AB, UK;
[2]School of Mining and Geosciences, Nazarbayev University, Astana, 010000, Kazakhstan
[3]Institute of Geology and Geophysics, Tashkent, 100164, Uzbekistan;
[4]Central-Asian Institute for Applied Geosciences, Bishkek, 720027, Kyrgyzstan;
[5]Central Asian Regional Glaciological Centre Under the Auspices of UNESCO, Almaty, 050010, Kazakhstan;
[6]Institute of Water Problems, Hydropower and Environment, Dushanbe, 734025, Tajikistan;
[7]Tien-Shan High Mountain Scientific Centre, Bishkek, 720033, Kyrgyzstan;
[8]Ulugh Beg Astronomical Institute of the Uzbekistan Academy of Science Tashkent, 100052, Uzbekistan;
[9]National University of Uzbekistan, Tashkent, 100174, Uzbekistan;
[10]Hydrometeorological Research Institute, Tashkent, 100052, Uzbekistan

Correspondence to: Zarina Saidaliyeva (z.saidaliyeva@pgr.reading.ac.uk)

Abstract. ~~The isotopic composition of precipitation in the mountains of four Central Asian countries (Kazakhstan, Kyrgyzstan, Tajikistan and Uzbekistan) was measured from 2019 – 2021 using 908 eEvent-based precipitation samples (n = 908) were collected at eight sites in 2019 – 2021, and supplemented by 7 monthly samples from Dushanbe (Tajikistan), with the isotopic composition determined by cavity ring-down spectroscopy (CRDS). thereby The measurements filling a gap in stable isotope data for the region. Regional and seasonal patterns of $\delta^{18}O$, δD and D*d-excess* were investigated, and Local Meteoric Water Lines (LMWL) was were derived using seven regression methods usingand both non-weighted and weighted precipitation. To derive LMWLs in the region, It is recommended that the the use of non-weighted Ordinary Least Squares Regression (OLSR) and Reduced Major Axis Regression (RMA) is recommended in general, but with methods can be applied across the region except in summer when the Precipitation-Weighted Least Squares Regression (PWLSR) method is recommended applied for summer (JJA) precipitation. An atmospheric back trajectory analysis and a mixing model were applied in combination for the first time, using the $\delta^{18}O$, δD and D*d-excess* data, to identify the atmospheric moisture source regions and quantify the relative to regional mountain precipitation. importance. The main distant sources were the Black and Caspian Seas region, Iran – eastern Mediterranean, and northern Kazakhstan – Siberia. The recycled moisture from the irrigated lower reaches of the Amu-Darya and Syr-Darya rivers, and from the study catchments, accounted for 29–71% of the atmospheric moisture reaching the observation points. In spring, summer and winter, in the Chon-Kyzyl-Suu catchment, up to 85% of the precipitation was estimated to be derived from local re-evaporation, most likely from Lake Issyk-Kul. These findings highlight the importance of moisture from terrestrial sources, especially irrigated land, in precipitation formation in Central Asia.~~ Over 900 event-based precipitation samples were collected in 2019–2021 in the Tien Shan and its foothills and analysed using cavity ring-down spectroscopy. δD and $\delta^{18}O$ values were highest in summer and lowest in winter, and annual cycles of d-excess varied between sites reflecting local conditions. The $\delta^{18}O$ and δD values increased from north to south in all seasons except autumn, and latitude was a statistically significant predictor of $\delta^{18}O$ and δD in the overall data set along with elevation in winter, and elevation and longitude in autumn. Elevation was a significant predictor of d-excess in all seasons, and local air temperature was a more important control over $\delta^{18}O$ and δD than precipitation depth. Local Meteoric Water Lines were derived using seven regression methods applied to non-weighted and weighted precipitation. Non-weighted Ordinary Least Squares Regression and Reduced Major Axis Regression methods are recommended overall, except for summer when the Precipitation-Weighted Least Squares Regression should be used, particularly in the south. Atmospheric back trajectory

Formatted: Font colour:Text 1
Formatted: paragraph,Font Alignment:Baseline
Formatted: Font colour:Text 1
Formatted: No underline,Font colour:Text 1
Formatted: Font colour:Text 1
Formatted: No underline,Font colour:Text 1
Formatted: Font colour:Text 1
Formatted: No underline,Font colour:Text 1
Formatted: Font colour:Text 1
Formatted: No underline,Font colour:Text 1
Formatted: Font colour:Text 1
Formatted: No underline,Font colour:Text 1
Formatted: Font colour:Text 1

and mixing model analyses were applied in combination to identify air-mass source-regions, and their relative contribution, to precipitation. Recycled moisture from irrigated land in the Amu Darya and Syr Darya basins and from the study catchments accounted for 29–71% of precipitation, depending on site and season. In the Chon-Kyzyl-Suu catchment, local re-evaporation from Lake Issyk Kul accounted for up to 85% of precipitation. These findings highlight the importance of moisture from terrestrial sources, especially irrigated land, for the formation of precipitation in the Tien Shan.

~~The main distant sources were the Black and Caspian Seas region, Iran – eastern Mediterranean, and northern Kazakhstan – Siberia.~~

1 Introduction

Atmospheric precipitation is the primary water source ~~of water which~~that contributes to river runoff in the mountains of Central Asia (CA), both directly and by sustaining seasonal snowpack and glaciers, whose meltwater maintains dry-season river flow ~~in the dry season~~. In CA, precipitation is characterised by strong spatial variability. ~~This variability is~~ due to large changes in elevation, ~~(~~from ~~about~~approximately 4~~7~~00 to 7000 m above sea level (a.s.l.) ~~up to 7000 m a.s.l.)~~ over relatively short distances, and the mountain ridge and valley positions in relation to the moisture-bearing flow (Lydolph, 1977; Aizen et al., 1997). Longer-term changes and interannual precipitation variability ~~in precipitation~~ affect all components of CA water resources (Shahgedanova, 2002; Jin et al., 2012; Aizen et al., 2017), and there is strong evidence for a decline in glacier area and negative glacier mass balance (Kutuzov and Shahgedanova, 2009; Farinotti et al., 2015; Severskiy et al., 2016; Kapitsa et al., 2020). ~~;~~ ~~t~~These changes are~~,~~ attributed ~~not only~~ to the observed air-temperature increase ~~, in temperature, but also~~and to prolonged negative precipitation anomalies observed in the 1970s-1980s (Shahgedanova et al., 2018; Hoelzle et al., 2019). ~~Future projections of precipitation in CA are characterised by strong uncertainty. Although overall, t~~Projections from the ~~The~~ Coupled Model Intercomparison Project Phase 6 (CMIP6) ~~projects~~ show an increase in annual precipitation in high mountain regions ~~in the future, the projected changes vary~~ with variation between regions and seasons ~~,~~ especially over the plains and foothills, and uncertainty remains about how these changes will be offset or enhanced by changes in evaporation and atmospheric circulation (Jiang et al., 2020). These ~~uncertainties~~uncertainties ~~is leads to a cascade of uncertainties~~are amplified in impact assessments using glacier mass balance, hydrological, water resource, and crop models. To reduce the uncertainties in the precipitation projections, ~~A~~a better understanding of ~~sources of~~ precipitation sources and moisture cycling, the links between changes in atmospheric circulation and precipitation, and ~~its~~of the precipitation response ~~s~~ to climatic warming, ~~is essential for water management and food production in the water- deficient regions~~ is needed ~~of CA~~ (Kaser et al., 2010; Immerzeel et al., 2020; Viviroli et al., 2020).

Analysis of the isotopic composition of precipitation ~~can be~~has been used to ~~constrain some of these uncertainties~~investigate precipitation sources and moisture cycling (Yoshimura, 2015; Putman et al., 2019; Jasechko, 2019), as the ~~. S~~stable isotopes of hydrogen and oxygen ~~are useful indicators of the meteorological~~describe water fractionation ~~history of atmospheric water from~~due to evaporation, ~~through~~ transportation and condensation, ~~to~~and precipitation ~~because these processes control fractionation which, in turn, controls isotopic composition~~. The ratios of heavy (^{18}O) to light (^{16}O) isotopes of oxygen ($\delta^{18}O$) and deuterium (D) to light hydrogen (^{1}H) ~~(δD)~~ and the relationship between δD and $\delta^{18}O$ in~~of~~ precipitation at the global scale, known as Global Meteoric Water Line (GMWL) and approximated by Equation (1), have been widely applied in hydrometeorology since the 1960s (Craig, 1961; Craig and Gordon, 1965):

$$\delta D = 8 \times \delta^{18}O + 10 \quad (1)$$

Rozanski et al. (1993) investigated δD and ~~oxygen~~ $\delta^{18}O$ relationships using the data from the Global Network of Isotopes in Precipitation (GNIP) sites and suggested that Local Meteoric Water Lines (LMWL) provide a better representation of isotopic composition of regional precipitation because they depend on latitude, continentality, altitude, and regional climatic anomalies.

Formatted: No underline,Font colour:Text 1
Formatted: Font colour:Text 1
Formatted: No underline,Font colour:Text 1
Formatted: Font colour:Text 1
Formatted: No underline,Font colour:Text 1
Formatted: Font colour:Text 1
Formatted: No underline,Font colour:Text 1
Formatted: Font colour:Text 1
Formatted: No underline,Font colour:Text 1
Formatted: Font colour:Text 1
Formatted: No underline,Font colour:Text 1
Formatted: Font colour:Text 1
Formatted: Font colour:Text 1
Formatted: No underline,Font colour:Text 1
Formatted: Font colour:Text 1
Formatted: No underline,Font colour:Text 1
Formatted: Font colour:Text 1
Formatted: No underline,Font colour:Text 1
Formatted: Font colour:Text 1
Formatted: No underline,Font colour:Text 1
Formatted: Font colour:Text 1
Formatted: No underline,Font colour:Text 1
Formatted: Font colour:Text 1

~~The relation of~~Relationships between ~~GMWL and to~~ LMWL~~s~~ help~~s to~~ identify regional characteristics and processes affecting precipitation (Wang et al., 2018; Putman et al., 2019). ~~It~~LMWLs ~~is~~are typically used together with the ~~concept of~~ deuterium excess (~~d~~d-*excess*)~~.~~; Equation (2) was developed by~~proposed as defined by~~ Dansgaard (1964) to define d-*excess* and is used to characterise moisture sources ~~of moisture where~~:

$$d\text{-}excess = \delta D - (8 \times \delta^{18}O) \quad (2)$$

The global average ~~d~~d-*excess* of precipitation is 10‰. In general, moisture recycling increases ~~and sub-cloud evaporation reduces~~ ~~d~~d-excess values and higher. ~~Increased~~ ~~d~~d-*excess* in precipitation ~~results from the significant~~signifies the addition of re-evaporated moisture from continental basins, while lower values ~~characterise~~signifie~~s~~ moisture originating from the oceans. This difference makes it possible ~~enables distinction~~ to ~~be made~~distinguish ~~between moisture~~precipitation ~~from distant~~originating over the distant oceanic ~~–~~sources and more local ~~–~~sources in the continental interiors (Araguás-Araguás et al., 2000; Pang et al., 2011; Aemisegger et al., 2014; Bershaw, 2018) particularly when ~~d~~d-*excess* is used in conjunction with atmospheric back-trajectory analysis (Wang et al., 2017, 2019; Bershaw, 2018). ~~Although non-equilibrium fractionation and evaporation are two major processes controlling D-excess, The s~~Ssub-cloud evaporation in a warm and dry air column ~~changes~~reduces ~~d~~d-*excess* ~~further obscuring the original vapor composition~~ (Friedman et al., 1962)~~,~~ and ~~d~~d-*excess* ~~in~~of ~~the~~ cloud condensate may be substantially different from the ~~d~~d-*excess* ~~in~~of precipitation samples collected at ~~the~~ ground ~~–~~level (Froehlich et al., 2008). ~~The sub-cloud evaporation effect is significant~~ especially in ~~the~~ arid regions ~~where precipitation intensity is low~~ (Juhlke et al., 2019). Isotopic composition and ~~d~~d-*excess* can also change with altitude (Bershaw, 2018; Natali et al., 2022; Yang et al., 2023) in response to ~~the due to~~ sub-cloud evaporation, ~~the~~ variations in distances travelled by a raindrop, and the transition from upwind ~~to the downwind rain shadow~~ slope, where~~by~~ lower temperature and higher humidity ~~cause lower~~supress evaporation ~~on the upwind slopes as~~ as orographic precipitation forms, to downwind rain shadow. While the

~~S~~sub-cloud evaporation and a shorter distance travelled by a raindrop are known to decrease d-excess values, ~~In contrast,~~ the rain shadow effect ~~tends to mitigate these decreases,~~ result~~s~~ing in higher d-*excess* ~~values~~. Consequently, d-*excess* serves as a valuable proxy for not only identifying precipitation sources but also for tracking changes in air mass moisture along its pathway.

~~Sub-cloud evaporation and a shorter distance travelled by a raindrop are known to increase D-excess values, while the rain shadow is known to reduce them, thereby making D-excess a useful proxy not only for precipitation sources but also for changes in airmass moisture over its pathway.~~

While the use of ~~isotopic analysis~~stable isotopes in hydrometeorology increases globally (Yoshimura, 2015; Aggarwal et al., 2016; Jasechko, 2019), knowledge about the isotopic composition of precipitation in CA (defined here as Kazakhstan (KZ), Kyrgyzstan (KG), Tajikistan (TJ), Turkmenistan, and Uzbekistan (UZ)) is limited. Currently, the ~~Global Network of Isotopes in Precipitation (~~GNIP~~)~~ database contains only seven measurements of δD and $\delta^{18}O$ from the precipitation samples collected in Tashkent, Uzbekistan (IAEA/WMO, 2015). This contrasts to extensive measurements in the Chinese Tien Shan (Pang et al., 2011; Wang et al., 2016b, 2018; Chen et al., 2021) where the Chinese Network of Isotopes in Precipitation (CHNIP) became operational in 2004 (Liu et al., 2014; Zhang and Wang, 2018).

The lack of CA precipitation isotope data prevents ~~constrains the~~ LMWL development ~~and as well as~~and limits the understanding and quantification of~~ying~~ the regional contributions to precipitation. In contrast to the Chinese Tien Shan where ~~the~~ events-based precipitation samples were analysed (Pang et al., 2011; Wang et al., 2016b, 2018; Chen et al., 2021), in CA, ~~ice-core~~ isotopic compositions from ice-cores taken from the Inylchek (Tien Shan) and Fedchenko (Pamir) glaciers only have been used to characterise moisture sources and regional atmospheric circulation patterns ~~in the central Tien Shan (Inylchek~~

Formatted: Font:Italic
Formatted: Font:Italic
Formatted: Font:Italic
Formatted: Font:Italic
Formatted: Font:Italic
Formatted: Font:Italic
Formatted: Font:Italic
Formatted: Font:Italic
Formatted: Font:Italic
Formatted: Font:Italic
Formatted: Font:Italic

~~Glacier; 42°09'N; 79°56'E , 5200 m a.s.l.) and Pamir (Fedchenko glacier; 38°15'N; 72°15'E, at two sampling sites with elevation 5206 and 5365 m a.s.l.) were used to characterise moisture sources and changes in regional atmospheric circulation patterns~~ (Aizen et al., 1996, 2004, 2009; Kreutz et al., 2003). Moisture sources for the Inylchek glacier were established broadly as the Atlantic Ocean, Mediterranean and Black Seas on the basis of $\delta^{18}O$ analysis combined with the catalogue of weather types (Aizen et al., 2004), whilst~~.~~ ~~M~~most precipitation over the Pamir originated in the Atlantic ~~according to~~ (Aizen et al., ~~(~~2009). The dominant moisture sources ~~of moisture~~ for the western Pamir were identified as the Mediterranean and Caspian Seas, which was ~~confirmed~~ further evidenced ~~by~~ by ~~the~~ high ~~*d*D~~ *excess* values of 20‰ measured in snow and ice cores ~~(by~~ Bershaw, ~~(~~2018). However, ~~in the western Pamir,~~ according to the event-based precipitation ~~samples~~ and trajectory~~ies~~ analyse~~is~~, ~~*d*D~~ *excess* in the western Pamir was lower at 13‰ leading to the conclusion that the Mediterranean contributed ~~about~~approximately 20% of the total moisture (Juhlke et al., 2019). This discrepancy may be due to the uncertainty in linking ice core samples to moisture trajectories, or because regional source signals are altered in CA along the long moisture transportation routes (Bershaw, 2018). ~~Insufficient data on precipitation isotopic composition mean current inferences are uncertain.~~

Formatted: Font:Italic

Formatted: Font:Italic

~~To fill the data and knowledge gaps, A~~a ~~s~~sampling programme~~field campaign was conducted between 2019 and 2021 by the Central Asia Research and Adaptation Water Network (CARAWAN) in five catchments located predominantly in the mountains (Fig. 1). Over 900 event-based precipitation samples were collected and processed, generating an extensive database of δD, $\delta^{18}O$, and *d*D *excess* values. The overall aim of the presented work is to determine the mountain precipitation source areas and to help achieve this, four objectives are defined to:~~o~~overall aim of the work is to determine the relative contributions of precipitation sources to the northern Tien Shan and western Pamir. ~~T~~The overall aim of the work is to determine the air-mass source-regions and trajectories of the precipitation falling over the northern Tien Shan with the purpose to improve knowledge of this aspect of the regional link between precipitation and water resources. To achieve the overall aim there are four objectives to:~~paper aims to~~ (i) ~~–~~ evaluate ~~precipitation stable isotope~~ the spatial and temporal variations in the isotopic composition of precipitation ~~in the mountains of CA~~; (ii) ~~characterise~~quantify the relationship between $\delta^{18}O$ ~~d18O~~ and ~~dD~~ δD ~~–isotope dependency on~~and ~~geographical~~ location, air ~~–~~temperature, and precipitation ~~amount of precipitation~~depth; (iii) ~~develop~~derive LMWLs ~~to aid future assessment of the relative contributions of different of water sources to streamflow, groundwater recharge, and isotope mass balance studies;~~, and (iv) establish a relationship between variations in isotopic composition of precipitation and air mass~~es~~ origin ~~and trajectories and its source regions~~. Objectives one, two and three are set to help better understand the atmospheric and geographical controls on precipitation isotope ratio variability in space and over time. ~~, and t~~The derivation of LMWLs (objective three) has the benefit of aiding the future assessment of the relative contributions of different water sources to streamflow, groundwater recharge, and isotope mass-balance studies. We combined a backward trajectory analysis with isotopologue data to explore the utility of the latter for determining the relative contribution of different air-mass source-regions to the regional mountain precipitation. To achieve the objectives and hence the overall aim, water stable isotopes were measured in precipitation samples between 2019 and 2021 by the Central Asia Research and Adaptation Water Network (CARAWAN) in five catchments located predominantly in the mountains (Fig. 1).

2 Data and methods

2.1 ~~Sampling points and characteristics of study area~~ Study area and sampling programme

Precipitation samples were collected in five river catchments:~~Sampling was conducted in five catchments of the rivers~~ Ulken Almaty (UA), Ala-Archa (AA), Chon Kyzyl-Suu (CKS), and Chirchik (CHK) ~~The eight sampling sites were located~~ in the

Tien Shan, and the Kofarnihon (KF) in the Pamir-Alai ~~mountains and their foothills~~ (Fig. 1a). CKS is located on the shores of Lake Issyk Kul, the largest fresh-water mountain lake in CA which does not freeze in winter. There is a smaller lake, which freezes in winter, in proximity to UA1 site. There were eight sampling sites six of which were ~~located~~ in the mountains between 1255 and 3277 m a.s.l. and ~~, with~~ two ~~sites located~~ in the foothills at lower elevations (Table 1).

In the UA, AA and CKS catchments in the north of the region, the Köppen climate classification is subarctic and tundra in the high mountains changing to humid-continental climate in the middle mountains and to the semi-arid grassland steppe as elevation decreases. In the CHK and KF catchments in the south, the Köppen climate classification changes with elevation from subarctic in the high mountains to humid-continental, then to a Mediterranean climate and to semi-arid grasslands and desert on the plains. ~~The regional climate is continental arid in the south and semi-arid in the north (Lydolph, 1977; Shahgedanova, 2002) with~~ The region is characterised by the strong seasonal~~ity~~ and altitudinal changes in temperature and precipitation (Fig 1~~b~~, c). In the foothills, mean July temperatures reach 24-26 °C and mean January temperatures vary between approximately –10 °C in the north and 5 °C in the south of the region. Annual precipitation ranges between 100 mm a^{-1} in the deserts of Uzbekistan and southern-western Kazakhstan to 1200 a^{-1} mm in the mountains. The location~~s~~ of the major mountain ranges is an important control over precipitation and, while the outer ranges receive ~~ample~~high precipitation during the wet season, intermontane basins are arid (Lydolph, 1977; Aizen et al., 1997). ~~In the southern part of the region, summer temperatures are high and precipitation is extremely low (Fig. 1 b, c).~~ Precipitation ~~starts~~ increases ~~ing~~ in October when regional atmospheric circulation is dominated by the westerly flow. ~~, and, a~~Across most of the region, precipitation ~~peaks~~ maxima occur in spring, ~~occurring earlier (~~in March – ~~,~~ April~~)~~ in the south and ~~later (~~April – ~~,~~ May~~)~~ in the north. At higher elevations in the northern Tien Shan, ~~the~~ precipitation ~~maximum is~~ peaks between May and July (Fig. 1c). In winter, the northern part of the region is dominated by the Siberian anticyclone and precipitation is low.

Formatted: Superscript

Formatted: Superscript

Formatted: Superscript

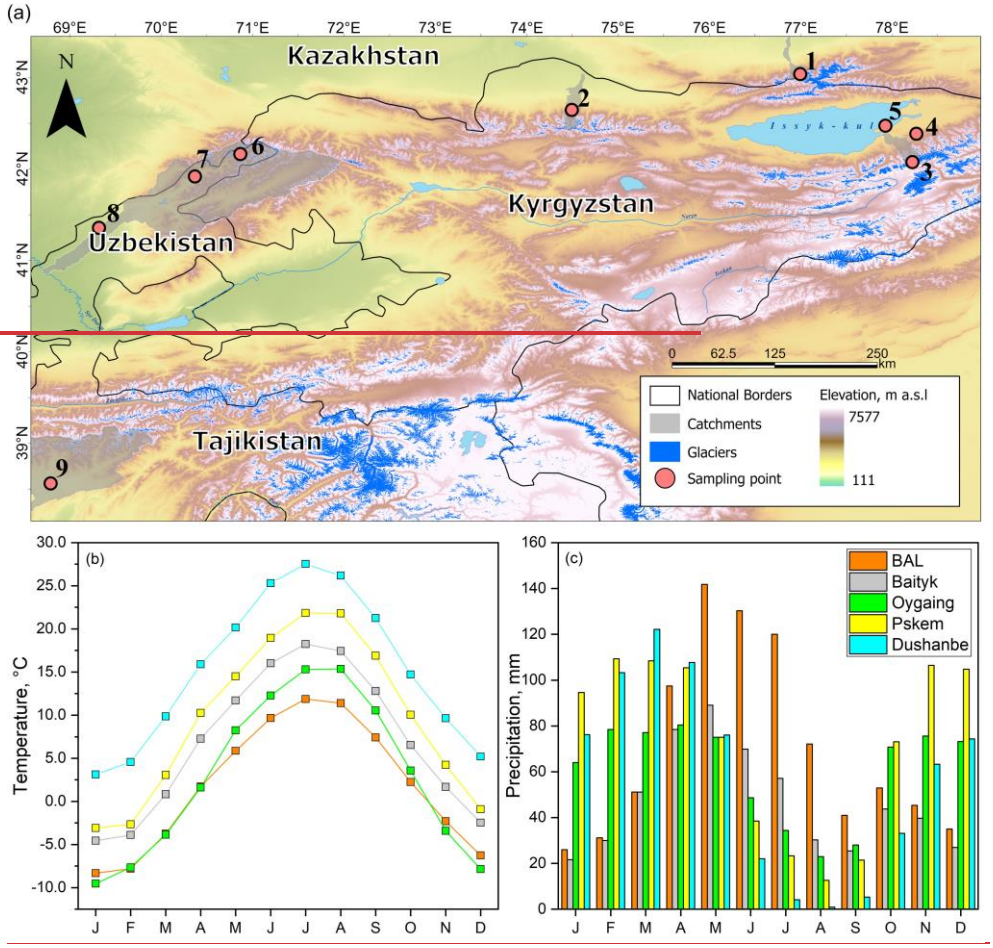
(a)
69°E
70°E
71°E
72°E
73°E
74°E
75°E
76°E
77°E
78°E
43°N
42°N
41°N
40°N
39°N
N
Kazakhstan
Kyrgyzstan
Uzbekistan
Tajikistan
Issyk-kul
1
2
3
4
5
6
7
8
9
0
62.5
125
250
km
National Borders
Catchments
Glaciers
Sampling point
Elevation, m a.s.l
7577
111
(b)
Temperature, °C
30.0
25.0
20.0
15.0
10.0
5.0
0.0
-5.0
-10.0
J
F
M
A
M
J
J
A
S
O
N
D
(c)
Precipitation, mm
160
140
120
100
80
60
40
20
0
BAL
Baityk
Oygaing
Pskem
Dushanbe

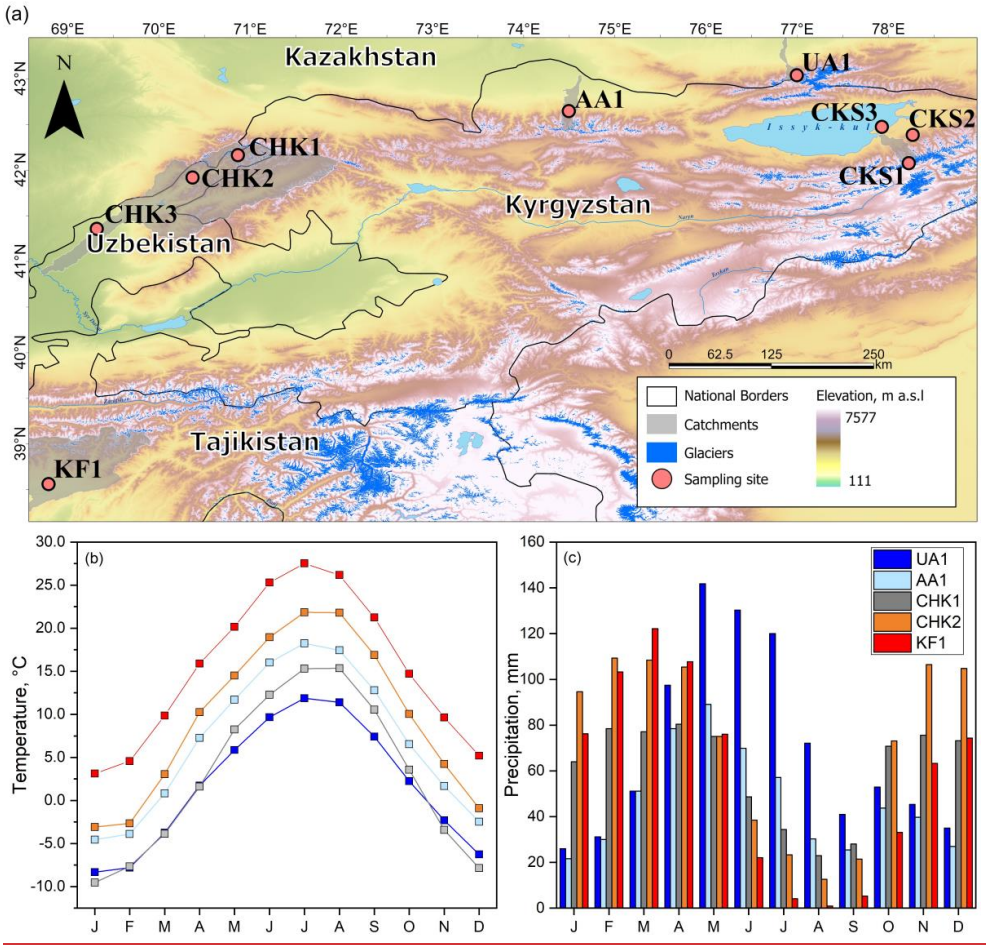

Figure 1: (a) Study area and locations of the sampling sites. Site numbering and details are given in Table 1. ~~: (UA1) Bolshoe Almatinskoe Lake (BAL), (AA12) Baityk, (CKS13) Karabatkak Glacier, (CKS24) Lesnoy Cordon, (CKS35) Tien-Shan High Mountain Scientific Centre (TSC), (CHK16) Oygaing (meteorological station Maydantal), (CHK27) Pskem, (CHK38) Tashkent, and (KF19) Dushanbe.~~ A Digital Elevation Model (DEM) derived from the Shuttle Radar Topography Mission (SRTM) is used as background (available from https://lpdaac.usgs.gov/about/citing_lp_daac_and_data). Glacier outlines are from the Global Land Ice Measurements from Space (GLIMS) database (Consortium, 2017). National borders and waterbodies are from ESRI ArcGIS Hub. (b) Mean monthly temperature and (c) mean monthly precipitation in the 1980-2015 period. ~~Sampling sites are numbered as in Table 1.~~

Field Code Changed

~~2.2 Event-based sampling of precipitation and design of laboratory isotopic analysis~~

Formatted: Normal, Justified,Line spacing: 1.5 lines

The event-based precipitation samples (n = 908) and meteorological data (daily air temperature~~,~~ ; depth ~~amount, and~~ type and duration of event-based precipitation) were collected between 2019 and 2021 ~~in five mountainous catchments at eight sampling sites generating, i~~In total, 908 event-based precipitation samples were collected ~~(Fig. 1a;~~ (Table 1). Seven samples of

cumulative monthly precipitation were collected in Dushanbe using a PALMEX rain sampler (http://www.rainsampler.com/portfolio-page/rain-sampler-rs1/).

Field Code Changed

Table 1: Characteristics of sampling sites (Fig. 1a) and details of the sampling programme. N is number of samples.

Site code~~number~~	Sampling sites	Catchment	Country	Lat (N)	Lon (E)	Elevation (m a.s.l)	Period	N	N with precipitation depth data
UA1	Bolshoe Almatinskoe Lake (BAL)	Ulken Almaty (UA)	KZ	43.04	76.99	2563	May 2019 - October 2021	338	332
AA1~~2~~	Baityk	Ala-Archa (AA)	KG	42.65	74.50	1588	July 2019 - May 2021	115	115
CKS1~~3~~	Karabatkak Glacier	Chon Kyzyl-Suu (CKS)	KG	42.16	78.27	3277	August 2019 - August 2021	37	35
CKS2~~4~~	Lesnoy Cordon		KG	42.19	78.20	2571	May 2019 - August 2021	117	114
~~5~~CKS3	Tien-Shan High Mountain Scientific Centre (TSC)		KG	42.35	78.02	1775	February 2020 - July 2021	29	-
CHK1~~6~~	Oygaing	Chirchik (CHK)	UZ	42.00	70.64	1490	Junuary 2020 - October 2021	196	196
CHK2~~7~~	Pskem		UZ	41.92	70.37	1255	November 2020 - July 2021	30	30
CHK3~~8~~	Tashkent		UZ	41.36	69.32	486	November 2020 - October 2021	46	46
KF1~~9~~	Dushanbe*	Kofarnihon (KF)	TJ	38.56	68.79	816	October 2018 - October 2019	7	6
			Total					915	874

*Cumulative monthly precipitation

Formatted Table

The event-based ~~Rainfall~~precipitation samples were collected using the~~traditional~~~~the~~ standard Tretyakov rain gauges immediately ~~-~~after the precipitation events by the trained meteorological observers who were ever present at the sites ~~daily 24 hours a day~~for the duration of the study period. ~~and precipitation depth was measured (observers were present at the station 24 hours a day for the duration of each year).~~ The rainfall samples were filtered using ~~the~~ 0.2 µm filters at the sampling sites and stored in 2 ml glass vials with screw caps pre-washed several times with the filtered rainwater. The s~~S~~nowfall samples were melted at room temperature, filtered ~~using the~~ (using ~~(~~0.2 µm~~)~~ filters~~)~~, and placed in the 2 ml glass vials. To avoid evaporation, all vials were sealed with Parafilm M (Bemis Company, USA, Part no. PM-992) and stored at 4ºC.

The samples were analysed using a Picarro Isotopic Water Analyzer (L2120-I) with measurement precision of ±0.6‰ and ±0.2‰ for δD and $\delta^{18}O$, respectively. ~~Error propagation for d-excess was calculated according to formula providing by Natali et al., (2022) and it resulted in an error of about ±2.5 ‰, by using the total errors of ±0.2 ‰ for $\delta^{18}O$ and ±0.6 ‰ for δD.~~ The sample analysis procedures and quality were ~~assessed and~~ certified by the International Atomic Energy Agency (IAEA) through the completion of a round-robin test using samples supplied by IAEA and according to the procedure and criteria outlined in Wassenaar et al. (2021). The error propagation for *d-excess* was calculated according to Natali et al. (2022) using the error values of ±0.2 ‰ for $\delta^{18}O$ and ±0.6 ‰ for δD and resulting in total uncertainty value of ±2.5 ‰.

Formatted: Font:Italic

The samples were injected into the analyzer seven times sequentially, and the first three measurements were discarded to avoid any memory effect from the previous samples. The remaining four measurements were checked for consistency using the

criterion of standard deviation not exceeding 1.5‰ and 0.15‰ for δD and $\delta^{18}O$, respectively. The final values were calculated as means of the four valid measurements. If four measurements, satisfying these conditions ~~could~~were not ~~be~~ obtained, the samples were re-measured and average of at least three valid measurements was recorded (52 samples). The isotopic ratios were recorded using delta-notation in *per mille* (‰) relative to the Vienna Standard Mean Ocean Water (V-SMOW):

$$\delta = \left(\frac{R_{sample}}{R_{standard}} - 1\right) \times 1000‰ \quad (3)$$

where R_{sample} and $R_{standard}$ are the isotope ratios $^{2}H/^{1}H$ or $^{18}O/^{16}O$ of the samples and the standard, respectively. Two primary Standard Mean Ocean Water (SMOW) and Standard Light Antarctic Precipitation (SLAP) and two secondary standards were used. The secondary standards were: (i) Tuyuksu Snow Melt Water (TSMW) collected from the Tuyuksu glacier (43.04°N; 77.08°E; 3780 m a.s.l.) ~~in the study area~~ located in proximity to the UA1 site with δD of –122.0‰ and $\delta^{18}O$ of –17.2‰, and (ii) commercially available Spring Water (SW) with δD of –55.0‰ and $\delta^{18}O$ of –8.5‰.

2.2. Quantifying links between isotopic composition of precipitation, geographical location, and local meteorological conditions

Stepwise regression was used to determine the relationship between isotopic composition of precipitation and latitude, longitude, and elevation. The $\delta^{18}O$ and δD values derived from all event-based samples collected at the individual sampling sites located between 38.56°N – 43.04°N, 68.79°E – 76.99°E, and 486 – 3277 m a.s.l. (Table 1) were the response variables.

The effects of surface air temperature and precipitation depth on mean monthly values of $\delta^{18}O$ and δD were examined using linear regression and the method of Dansgaard (1964). The latter suggested that a difference between isotopic ratios of $\delta^{18}O$ averaged over warm (May – October) and cold (November – April) periods are indicative of the control by either by local temperature or precipitation amount over isotopic ratios. Positive values of the $\delta^{18}O$ difference are typical of the high- and mid-latitude continental regions and indicate a strong surface air temperature control over the isotopic composition of precipitation.

2.3~~2~~ Local Meteoric Water Line (LMWL)

There are two approaches to defining LMWL. The first approach ~~one gives~~assigns equal weighting to all data points regardless of the amount of precipitation they represent and is used. ~~This approach applies potentially increases uncertainty in the interpretation of results~~ to evaluate the atmospheric and hydrometeorological processes ~~that govern~~controlling the isotopic composition of precipitation. ~~because~~However, ~~while~~ samples obtained from smaller precipitation events tend to have lower *d~~D~~-excess* due to the sub-cloud evaporation leading to sample enrichment ~~while~~in comparison to samples obtained from the heavy precipitation events ~~tend to be~~ which are more depleted (Hughes and Crawford, 2012; Crawford et al., 2014). To overcome this problem and to represent hydrologically significant precipitation, which is important for local hydrological applications, weighted precipitation ~~is~~is~~was~~ used. This method requires data on precipitation depth ~~which were available in this study~~ (Table 1). Both approaches were used for comparison and to produce recommendations on the LMWL development in the study region considering that precipitation depth may not be available in other projects.

Ordinary Least Squares Regression (OLSR) was used to define LMWL ~~with~~from the unweighted samples (n=915; Table 1). Precipitation depth~~amounts~~ ~~were~~was recorded for 874 samples (Table 1) which were used in the precipitation-weighted analysis. Six regression methods were applied to the event-based precipitation samples: three non-weighted (OLSR, Reduced Major Axis Regression (RMA), and major axis regression (MA)) and three precipitation-weighted (Precipitation-Weighted

Formatted: Font:(Default)Times New Roman, 10 pt, English(United Kingdom)
Formatted: Font:(Default)Times New Roman, 10 pt, English(United Kingdom)
Formatted: Font:(Default)Times New Roman, 10 pt, English(United Kingdom)
Formatted: Heading2, Left, Line spacing: single
Formatted: Not Highlight
Formatted: Not Highlight
Formatted: Not Highlight
Formatted: Not Highlight
Formatted: Not Highlight
Formatted: Not Highlight
Formatted: Not Highlight
Formatted: Not Highlight
Formatted: Not Highlight
Formatted: Not Highlight
Formatted: Not Highlight
Formatted: Not Highlight
Formatted: Not Highlight
Formatted: Not Highlight
Formatted: Not Highlight
Formatted: Not Highlight
Formatted: Not Highlight
Formatted: Not Highlight
Formatted: Not Highlight
Formatted: Not Highlight
Formatted: Not Highlight
Formatted: Font:10 pt

Least Squares Regression (PWLSR), Precipitation-Weighted Reduced Major Axis Regression (PWRMA), and Precipitation-Weighted Major Axis Regression (PWMA)) (Hughes and Crawford, 2012; Crawford et al., 2014). The Local Meteoric Water Line Freeware (available at http://openscience.ansto.gov.au/collection/879) was used in all calculations. The software calculates the following parameters: slope of regression line (a), standard deviation of the slope (sa), intercept of regression line (b), standard deviation of the intercept (sb), average value of the sum of the squared errors of three methods, either OLSR, RMA and MA ~~(or~~or three precipitation ~~weighted)~~ regressions, root mean Sum of Squared Errors (RMSSE), which allow inter-comparison of ~~the~~ different regression methods. The proximity of the RMSSE values to 1.0 was used as an indicator of the method suitability for the analysed data set. The t-test was applied to evaluate statistical significance of a difference between OLSR and each other regression method.

2.~~4~~3~~4~~ Back trajectory modelling and cluster analysis using HYSPLIT

Isotopic composition of precipitation is determined by the combination of the origin of moisture, ~~and~~ history of atmospheric water transport, and local conditions (Rozanski et al., 2013). To evaluate the controls of atmospheric circulation over the isotopic composition of precipitation and characterise its geographical sources, $\delta^{18}O$, δD, and ~~*d*D~~ *excess* values were used in conjunction with the three-dimensional atmospheric back trajectory analysis. ~~using t~~The HYbrid Single-Particle Lagrangian Integrated Trajectory (HYSPLIT) model (version 5.2.0) ~~run~~ with the Global Data Assimilation System (GDAS) meteorological input (Draxler and Rolph, 2013; Stein et al., 2015; Rolph et al., 2017) ~~was used~~. HYSPLIT, which has a ~~has a~~ horizontal resolution of 1°, ~~and HYSPLIT~~ was run for each precipitation event registered at ~~sampled at sampling points (latitude longitude and elevation were used as input parameters for final destination point of trajectory)~~ UA1~~BAL (UA)~~, ~~Lesnoy Cordon (CKS)~~CKS2, ~~Baityk (AA)~~AA1, and ~~Oygaing (CHK)~~CHK1 (Table 1) using latitude, longitude, and elevation of the sites as input parameters. All sites were located between 1255 and 2571 m a.s.l. The use of site elevation as starting point is justified because in the region, most moisture in the air column is contained between 1500 and 3000 m where lifting condensation level is positioned and where precipitation forms (Chen et al., 2024; Zongxing et al., 2016). ~~The starting time of each back trajectory was defined as the closest hour of the precipitation event start, and t~~The length of integration was 120 hours because uncertainty in the calculation of trajectories increases with time afterwards (Draxler and Rolph, 2013). ~~We experimented with trajectories of different duration finally limiting it to 120 hours to minimise uncertainty in HYSPLIT modelling which increases strongly after this period of time (Draxler and Rolph, 2013). The mean water vapour residence time in the atmosphere is estimated by many studies as 8 - 10 days although its~~ The global median value of water vapour residence time in the atmosphere is estimated ~~was estimated~~ as approximately five days (120 hours) although several studies estimate it as 8 - 10 days (Van Der Ent and Tuinenburg, 2017). ~~Therefore, limiting the length of back trajectories to 120 hours is not an issue for the shorter local and Aral Sea region trajectories. However, the identification of source regions in the westerly group (1-3) could be potentially affected especially in winter when water vapour residence time increases over the continental interiors in the Northern Hemisphere compared to summer (Van Der Ent and Tuinenburg, 2017).~~

In line with previous studies (Jorba et al., 2004; Wu et al., 2015; Pérez et al., 2015; Bagheri et al., 2019; Kostrova et al., 2020) and to comply with the HYSPLIT cluster analysis function requirements, single trajectories were calculated instead of trajectory ensembles, potentially introducing uncertainty. The starting time of each back trajectory was defined as the hour closest to the start of precipitation event. The median duration of precipitation events was 240 minutes. A comparison between trajectories calculated for the start and the end of precipitation events exceeding 660 minutes (90th percentile) was performed. The differences between the coordinates of their point of origin was within the HYSPLIT ~~accuracy~~resolution.

The generated back trajectories were grouped using cluster analysis based on minimizing distance and maximizing difference between clusters with distinct trajectories (Dorling et al., 1992). The ~~and performed using the~~ HYSPLIT 5.2.0 built-in cluster

Field Code Changed

Formatted: Not Highlight

Formatted: Font:Italic

Formatted: Font:10 pt, Fontcolour:Auto

Formatted: Fontcolour:Auto

Formatted: Font:10 pt, Fontcolour:Auto

Formatted: Fontcolour:Auto

Formatted: Font:10 pt, Fontcolour:Auto

Formatted: Fontcolour:Auto

Formatted: Fontcolour:Text 1

Formatted: Not Highlight

Formatted: Superscript

analysis function (available at https://www.ready.noaa.gov/HYSPLIT_hytrial.php) was used to derive clusters for ~~for~~ the ~~selected four~~UA1, CKS2, AA1 and CHK1 ~~sampling~~ sites. Total spatial variance (TSV), defined as ~~the~~ sum of the spatial variances of all clusters, was~~is~~ used to determine the optimal number of clusters. The percentage of change in TSV was plotted against the number of clusters and~~.~~ ~~T~~the first large increase in the change of TSV was taken as an indicator of the final number of clusters (Wilks, 1995; Kostova et al., 2020).

~~Trajectories calculated for all events observed at each site throughout the year were grouped.~~ Isotopic ratios and *d*~~D~~-*excess* values were initially analysed for the clusters generated for each site and season. However, many trajectory clusters generated for different sites were similar (e.g., the 'W~~w~~est~~erly~~' ~~trajectory~~ cluster was generated for each site; see Figure~~.~~ ~~6~~7 further in the text). Splitting the data by season for each site resulted in a small number of members in each cluster. To overcome this problem, similar trajectory clusters from different sites were merged ~~to form 'synoptic circulation groups'~~. Some of the ~~groups~~ clusters included data from all sites (e.g. W~~w~~est~~erly~~) while others were limited to a smaller number of sites. ~~Analysis of the~~ Isotopic ratios and *d*~~D~~-*excess* ~~was then performed~~were averaged by ~~the 'synoptic circulation groups' and~~ cluster and meteorological seasons. Analysis of variance (ANOVA) and pairwise t-tests were used to test whether the differences between $\delta^{18}O$, δD, and *d*~~D~~-*excess* values attributed to different ~~groups~~clusters were significant at ~~a~~ 95% confidence level.

2.5~~4~~5 Quantifying relative contributions of the ~~identified moisture sources~~trajectory sources to total precipitation.

~~Source regions of moisture and its transport pathways were characterised using the cluster analysis of the HYSPLIT back trajectories.~~ The proportional contributions of ~~multiple~~ the trajectory sources to the total precipitation were quantified using a linear mixing model whereby two isotopic signatures ($\delta^{18}O$ and δD) enable partitioning of the total precipitation between three sources (Phillips and Gregg, 2001). ~~The isotopic signatures of precipitation samples attributed to a source, identified via the cluster analysis of back trajectories, were determined and mean signature values of $\delta^{18}O$ and δD were calculated for each source and their mixture.~~ Fractional contributions were calculated using Equations (4) and (5) (Phillips and Gregg, 2001):

$$\delta_P = f_A\delta_A + f_B\delta_B + f_C\delta_C \quad (4)$$

$$f_A + f_B + f_C = 1 \quad (5)$$

where f_A, f_B and f_C are fractional contributions of different ~~moisture~~trajectory ~~sources~~groups to local precipitation, δ_A, δ_B, δ_C are ~~their~~ isotopic ~~signature~~ values of each group by season, and δ_P is seasonal mean isotopic value for all precipitation events during the sampling period. The software *IsoError Version 1.04* (available at http://www.epa.gov/eco-research) (Phillips and Gregg, 2001)) was used to apply the mixing model.

~~Although~~ T~~t~~he mixing model was limited to a maximum of three contributing trajectory sources (Equations 4 - 5) but ~~For each site, between three and~~up to ~~five clusters~~clusters of back trajectories were identified~~.~~. The number of clusters ~~similar trajectory clusters from different sites were~~was reduced ~~merged~~ to form ~~five~~three trajectory groups for different seasons ~~(Section 2.4; Fig.6)~~using t~~.~~he following~~Three~~ criteria: ~~were used for merging the identified clusters into groups~~ (i) direction of travel; (ii) distance travelled; and (iii) whether local circulation trajectories remained within the catchment boundaries. Clusters 1, 2 and 3 were merged to form a single (West) group~~To reconcile the number of synoptic groups with the three-component models, Groups 1, 2, and 3 were merged (westerly group)~~ because, despite the differences in directions, they were associated with the long-distance transport along the peripheries of depressions originating over the Atlantic. ~~(Section 3.3).~~ Statistical significance of differences between $\delta^{18}O$, δD, and *d-excess* values associated with different groups ~~the clusters and groups (Fig. 7; S2-3)~~ were assessed using ANOVA.

Field Code Changed

Formatted: Font:(Default)Times New Roman, 10 pt, English(United Kingdom)

Formatted: Font:(Default)Times New Roman, 10 pt, English(United Kingdom)

Formatted: Font:(Default)Times New Roman, 10 pt, English(United Kingdom)

Formatted: Font:10 pt, English(United Kingdom)

Formatted: Font:Italic

Formatted: Font:Italic

Formatted: Font:Italic

Field Code Changed

3 Results

3.1 Seasonal and spatial variability in δD and $\delta^{18}O$.

The descriptive statistics of δD and $\delta^{18}O$ derived from ~~all~~the ~~–~~event~~-~~based precipitation ~~events~~ at each catchment are summarized in Figure 2 and ~~in~~ Table S1 (where data are shown for each sampling site and for three types of precipitation: snow, rain and mixed)~~ over the entire period of sampling programme~~. The ~~total means values of~~ $\delta^{18}O$ and δD means and standard deviations for all events between 2019 and 2021 were ~~-~~8.6±6.5‰ and ~~-~~56.1±50.1‰, respectively. ~~-~~Rain samples (n=528) were characterized by the higher mean $\delta^{18}O$ and δD values of –4.9‰, and −28.1‰, respectively, whereas snow samples (n=260) have lower mean $\delta^{18}O$ and δD values of −15.4‰ and −110.7‰, respectively (Table S1~~;~~ ~~and Fig. 4 further in the text~~). Variability in the snow ~~data~~ sub-set was higher than in the rain ~~data~~ sub-set with standard deviations of ±5.5‰ ($\delta^{18}O$) and ±44.6‰ (δD) for snow and ±4.3 ‰ ($\delta^{18}O$) and ±30.0‰ (δD) for rain. ~~This is because in winter, day-to-day temperature fluctuations, associated with changing synoptic conditions, are stronger than in summer with mean temperature changes between two consecutive days of 4ºC (Shahgedanova, 2002).~~ The mixed precipitation data set, based on 120 samples, showed intermediate values of $\delta^{18}O$ of −9.7‰ and δD of −61.7‰. Contrary to the expectation that standard deviations of the mixed precipitation isotopic ratios should be the highest, reflecting different proportions of solid and liquid content of precipitation in a sample, their values were the lowest for $\delta^{18}O$ and broadly the same as for rain for δD (Table S1).

Clear seasonal cycles were observed in δD and $\delta^{18}O$ values in each catchment where isotopic ratios were higher in summer and lower in winter (Fig. 2a, b; Table S1). In the event-based precipitation samples, $\delta^{18}O$ and δD values varied widely from –33.6 to 8.6‰ and from –258.8 to 45.2‰, respectively (Fig. 2a, b). Both $\delta^{18}O$ and δD showed larger variability in those months when snow and mixed precipitation were observed, namely between November and March in more southerly CHK catchment and in April-May and November in other catchments (Fig.2a, b; Table S1). The CHK3 site (17% of all CHK samples; two samples only in JJA) was located at 486 m a.s.l. enhancing the difference with other catchments and sites (Fig. 3). Between late spring and early autumn, the between-sample variability was reduced, and the standard deviations were lower except for the higher-elevation and more northerly catchments, i.e. UA and AA (Fig. 2a, b).

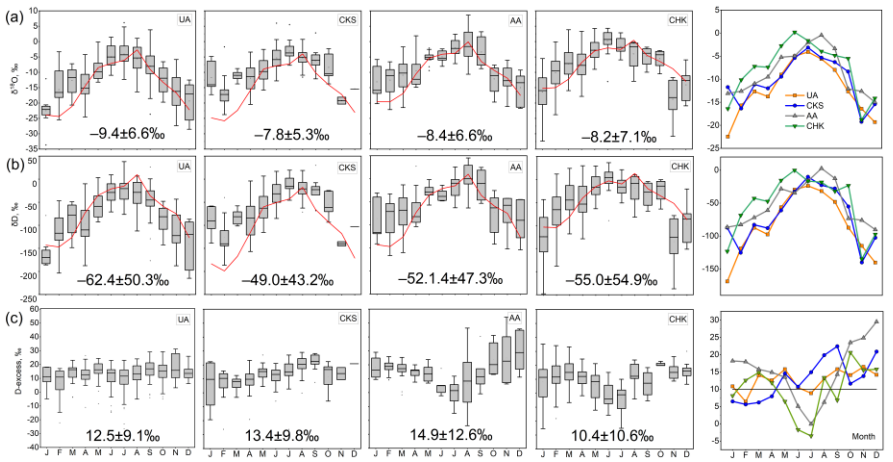

Formatted: Heading1, Left

Formatted: Font:Not Bold, Not Highlight

Formatted: Font:Not Bold

Formatted: Font:Not Bold, Not Highlight

Formatted: Font:Not Bold

Formatted: Font:Not Bold

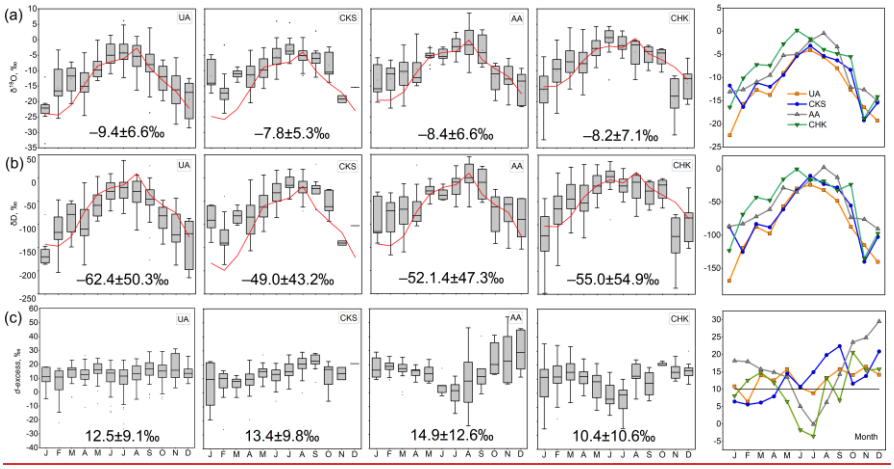

Figure 2: Boxplots of (a) $\delta^{18}O$, (b) δD, and (c) ~~d~~*d-excess* in precipitation collected at the four catchments (see Fig. 1 and Table 1 for locations of catchments and number of samples) between 2019 and 2021 (left panel) and mean monthly d-excess values (right panel). Precipitation was sampled at three sites in CHK and CKS and data from all sites are included. Annual mean values ± standard deviation calculated for the 2019 – 2021 period are shown. The ~~Straight~~horizontal~~:~~ line in (c; right panel) shows the global mean ~~d~~*d-excess* ~~value~~. The red line shows data from the Waterisotopes Database (Bowen, 2022). The Waterisotopes Database data were averaged over all sampling locations ~~for~~ in ~~catchments with more than one sampling site (~~CKS and CHK~~)~~.

Formatted: Font:Italic

Formatted: Font:Italic

Formatted: Font:Not Italic

~~Clear seasonal cycles were observed in δD and $\delta^{18}O$ values in each catchment where precipitation is enriched in heavy isotopes in summer and depleted in winter (Fig. 2a, b; Table S1). The stable isotope composition of event-based precipitation varied widely from −33.6 to 8.6‰ for $\delta^{18}O$ and from −258.8 to 45.2‰ for δD, with overall means of −8.6 ± 6.5‰ and 56.2 ± 50.2‰, respectively (Fig. 2a, b). Hydrogen is more susceptible to fractionation and less stable than oxygen and, therefore, δD exhibits greater variability than $\delta^{18}O$ (Hornberger, 1999; Gat, 2010). Both isotopes d18O and dD showed larger variability in those months when snow and mixed precipitation are observed, namely between November and March in more southerly CHK catchment and in April–May and November in other catchments (Fig.2a, b; Table S1). The CHK data contain samples from Tashkent, which is located on the arid plain at 486 m a.s.l. (Table 1). These account for 17% of all CHK samples. Only two samples were collected in summer in CHK3Tashkent, but these two samples make the difference with other sites more pronounced (Fig. 3). Between late spring and early autumn, between-sample variability is reduced, and the standard deviations are lower except for the higher-elevation and more northerly catchments: UA and AA (Fig. 2a, b). The observed seasonal cycles are generally consistent with the previous global interpolation of precipitation isoscapes (Bowen and Revenaugh, 2003; Bowen et al., 2019) and the global high-resolution isotope precipitation data (Terzer-Wassmuth et al., 2021). However, these previous interpolated estimates significantly underestimate the precipitation isotopic ratios in the study region in the cold period (Fig. 2a, b) due to the lack of data currently available in the two databases. For example, the annual mean difference between measured and derived from database (Fig. 2) varies from −0.3‰ (CHK) to 4.8‰ (CKS) for $\delta^{18}O$ and from −6.7‰ (CHK) to 37.4 (CKS) for δD but reaches 10.1‰ (CKS) for $\delta^{18}O$ and 52.5‰ (AA) for δD in winter (Fig.2a, b; S1).~~

The relationship between isotopic precipitation composition and latitude, longitude and elevation were quantified by the following equations, derived using all available samples:

$$\delta^{18}O = 36.3 - 1.18Lat + 0.07Lon - 0.00001E \quad (6)$$

$$\delta D = 342 - 10.75Lat + 0.73Lon - 0.002E \quad (7)$$

where Lat is latitude (°), Lon is longitude (°), and E is elevation (m a.s.l.). Regression equations for four meteorological seasons are shown in Table S2. Latitude is the only statistically significant predictor of both $\delta^{18}O$ and δD in the overall data set ($p < 0.01$) while relationships with longitude and elevation were not statistically significant. Elevation was the only significant predictor of $\delta^{18}O$ and δD in winter. Elevation and longitude were significant predictors in autumn ($p < 0.05$).

Three sites with an elevation difference of more than 800 m a.s.l. in CHK and CKS allowed examination of elevation gradients in isotopic ratios and *d-excess* which were calculated using the lowest and the highest sampling points for which data were available (Table 1). For both $\delta^{18}O$ and δD, the gradients were highest in summer but not consistent between CKS and CHK (Fig. 3). Very few samples were available for the CHK3 (city of Tashkent) site located in the foothills and isotopic ratios were not consistent with the high temperatures registered at this site. ~~Stepwise regression was used to determine the relationship between isotopic precipitation composition and latitude, longitude and elevation (Table S2). The $\delta^{18}O$ and δD derived from all event-based samples collected at the individual sampling sites located between 38.56°N – 43.04°N, 68.79°E – 76.99°E, and 486 – 3000 m a.s.l (Table 1) were the response variables. The regression equations, derived using all available samples, were:~~

~~$$\delta^{18}O = 36.3 - 1.18Lat + 0.07Lon - 0.00001E \quad (6)$$~~

~~$$\delta D = 342 - 10.75Lat + 0.73Lon - 0.002E \quad (7)$$~~

~~where Lat is latitude (°), Lon is longitude (°), and E is elevation (m a.s.l.).~~

~~Statistically significant relationships between both $\delta^{18}O$ and δD and latitude ($p < 0.01$) were found. Relationships with longitude and elevation were not statistically significant in the overall data set. Regression equations for meteorological seasons are shown in Table S2. In winter, elevation was the only predictor significantly correlated with the isotopic ratios while, in autumn, elevation and longitude were significant ($p < 0.05$). Three sites with an elevation difference of more than 800 m a.s.l. in CHK and CKS allowed examination of elevation gradients in isotopic ratios and *d-excess* which were calculated using the lowest and the highest sampling points for which data were available (Table 1). For both $\delta^{18}O$ and δD, the gradients were highest in summer but not consistent between CKS and CHK (Fig. 3). Very few samples were available for the lowest stations and isotopic ratios at Tashkent were not consistent with the high temperatures registered at this site.~~

~~The effects of surface air temperature and precipitation depth on mean monthly values of $\delta^{18}O$ and δD were examined using correlation analysis and the method of Dansgaard (1964). The latter suggested that a difference between isotopic ratios of $\delta^{18}O$ averaged over warm (May-October) and cold (November-April) periods can indicate control by local temperature or precipitation amount on isotopic ratios. Positive values of the $\delta^{18}O$ difference are typical of the high- and mid-latitude continental stations and indicate a strong surface air temperature contribution to the precipitation isotopic composition. In the study region, T~~the indices, derived from the application of Dansgaard (1964) method confirmed the links between isotopic ratios and temperature evident from Figure 2. The indices were positive, ranging between 7.0‰ in CKS and 8.6‰ in UA (Table S3) therefore demonstrating a strong temperature effect and lesser influence of precipitation amount on isotopic ratios. For the whole data set, ~~C~~coefficients of determination for the ~~regression equations linking the~~ event-based values of δD and $\delta^{18}O$ and air temperature (measured at the sampling sites) were 0.56 and 0.54, respectively (Equations 8 – 9) ranging between

Formatted: Highlight

Formatted: Not Highlight

ranged between 0.46 and 0.66 for all measurements (Equations 8-9) and for the individual sampling sites (Table S4). They and were statistically significant at the 95% confidence level – except Tashkent CHK3. The $\delta^{18}O$ and δD changed by 0.62‰ and 4.68‰ per one degree temperature, respectively, for the whole data set. The highest coefficients were obtained for the Baityk (AA) AA1 and Oygaing (CHK) CHK1 sites (0.66 and 0.64, respectively) and the lowest (0.27) for CHK3 Tashkent. The $\delta^{18}O$ and δD changed by 0.62‰ and 4.68‰ per one degree temperature, respectively, for the whole data set. The highest gradients were observed at CHK1 Oygaing (0.74‰ and 5.50% per 1°C) and the lowest at CHK3 Tashkent (0.32‰ and 2.46% per 1°C) (Table S4).

$$\delta^{18}O = 0.62t - 10.61, R^2 = 0.56 \quad (8)$$

$$\delta D = 4.68t - 71.64, \ R^2 = 0.54 \quad (9)$$

where *t* is air temperature (°C) at the sampling sites.

There was no statistically significant correlation between isotopic ratios and daily amount of precipitation depth in the study region.

3.2 *d*D *excess* variations over the region and elevation effects

Figure 2c shows annual cycles of *d-excess*. The mean seasonal *d-excess* values ranged between 13.07‰ and 15.15‰ in SON, DJF and MAM. In JJA, the mean *d-excess* value was 12.41±10.26 8.58‰ (Figure 2c). Figure 2c shows annual cycles of *d*D *excess*. In the AA and CHK catchments, minimum *d*D *excess* values were are observed in June-July (when mean monthly values were negative) increasing in winter DJF (AA), and spring MAM and autumn SON (CHK). In UA and CKS, seasonal cycles are were less pronounced (UA) or different, with a maximum in August – September (CKS). In CKS and UA, sites are in proximity to lakes Issyk Kul (Fig. 1) and Bolshoe Almatinskoe (BAL), respectively. The lake effect is evident in the cold season due to the contrast between an enhanced contribution of heavier water vapour from the lake and lighter vapour delivered by the cold air masses (Bowen et al., 2012; Xiao et al., 2017; Minder et al., 2020). This effect results in higher isotopic enrichment ratios of precipitation and lower *d*D *excess* values. In CKS, located on the shores of Lake due to Issyk Kul (which does not freeze in winter in contrast to BAL), *d*D *excess* was is below 10‰ between January and April.

In spring, *d*D *excess* values in excess of greater than above in excess 1 of 1 0‰, indicate a strong contribution of recycled moisture to precipitation (Koster et al., 1993; Bershaw, 2018), and are were observed in all catchments in spring (except CKS in March – April) and autumn – early winter in line with the occurrence of the wet season (Fig. 1). In the AA catchment, values more than over 10‰ are were observed throughout the cold season between September and May. Values more than 20‰, indicating strong re-evaporation (Fröhlich et al., 2001; Bershaw, 2018), and are were evident between October and December in the AA catchment and in the individual months in the same period in CHK (October) and CKS (September, December). The particularly high mean monthly value reaching s reaching 29.5‰ was ere recorded in the AA catchment in December although this calculation is based on seven samples (Table S1).

The timing of low *d*D *excess* values, indicative of the sub-cloud evaporation effect (Fröhlich et al., 2001; Bershaw, 2018), varies between catchments (Fig. 2c; Table S1). Negative mean monthly *d*D *excess* values were observed in CHK and AA in May to September reaching -3.5‰ in July in CHK. Low precipitation amounts and higher temperatures in CHK in summer (Fig. 1) enhance negative *d*D *excess* values and the elevational profiles of *d*D *excess* are complex (Fig. 3c).

Formatted: Font:Italic
Formatted: Not Highlight
Formatted: Not Highlight
Formatted: Font:Italic
Formatted: Font:Italic
Formatted: Font:Not Italic
Formatted: Font:Italic

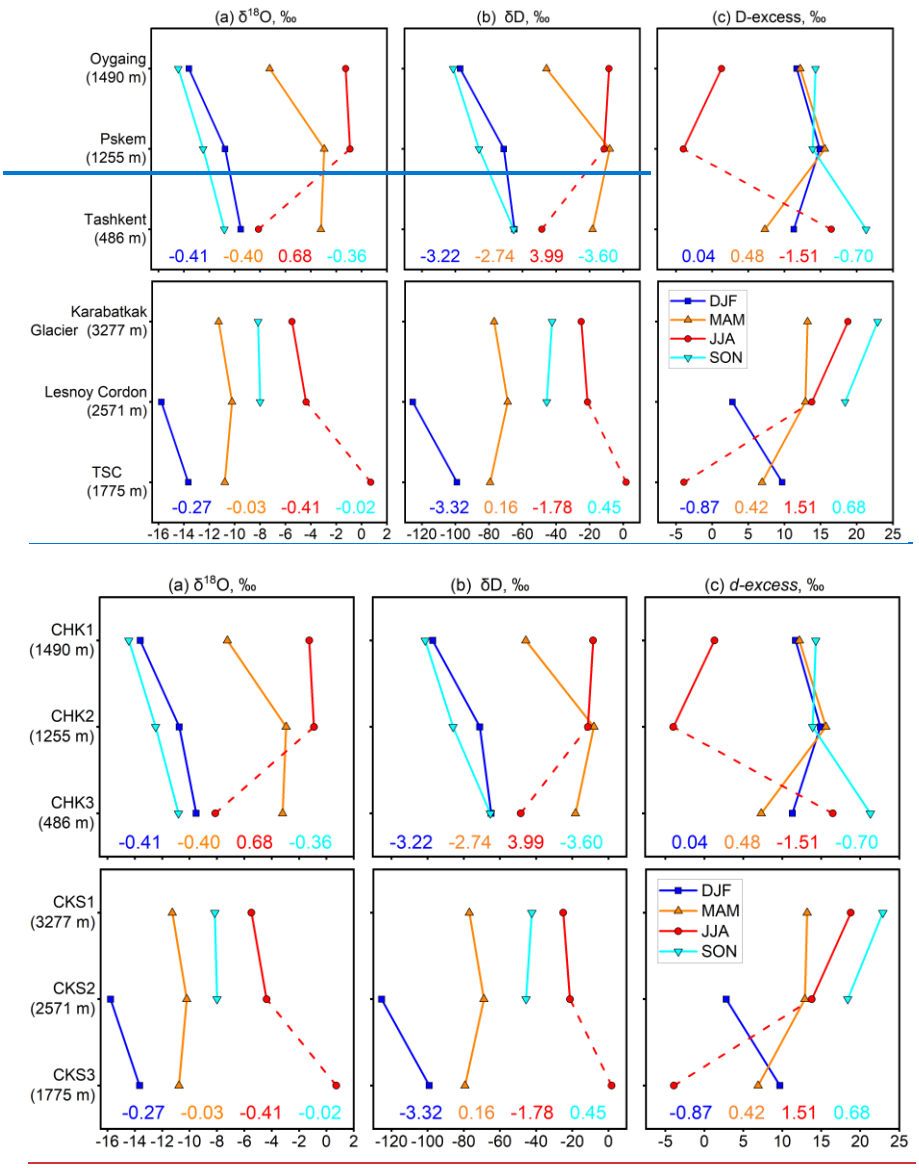

Figure 3: Changes with elevation in (a) $\delta^{18}O$, (b) δD, and (c) *d*~~D~~-excess by season in CHK (upper panel) and CKS (bottom panel). Dashed lines indicate small number of samples and low precipitation per event in CHK3~~-Tashkent~~ and CKS3~~TSC~~. Numbers show seasonal values of elevational gradients (‰ per 100 m).

Figure 3 shows elevational profiles of *d-excess*. ~~The emerging patterns of changes in *dD-excess* with elevation were inconsistent between sites and seasons (Fig. 3) partly because of the complex controls on *dD-excess* and, potentially, because~~

Formatted: Not Highlight

Formatted: Font:Italic, Not Highlight

Formatted: Not Highlight

~~precipitation events were not always observed on the same days at different sites in the same catchment.~~ ~~The clearest pattern~~ ~~was observed i~~In CKS, ~~in JJA where~~ ~~*d*D~~-*excess* values increased with elevation~~altitude~~ from –3.9‰ (n=3) at CKS~~HK~~3 ~~TSC~~ located at 1755 m a.s.l. to 18.9‰ (n=28) at the CKS1~~Karabatkak glacier~~ (3277 m a.s.l.) in JJA ~~indicating the advection of recycled moisture at higher elevations, progressive orographic moisture removal, and reduced sub-cloud evaporation typical of the mountain stations due to a smaller distance between the ground and the cloud base (Fröhlich et al., 2001; Bershaw, 2018)~~. Similar altitudinal profiles were observed in MAM albeit with a reduced gradient (6.9‰ and 13.2‰ at CKS3~~TSC~~ and CKS1~~Karabatkak~~, respectively) and in SON when data were available for the CKS2~~Lesnoy Cordon~~ (2571 m a.s.l.) and CKS1 ~~Karabatkak~~ sites only (Fig. 3c). ~~Small gradients may be attributed to the reduced sub-cloud evaporation in both spring and autumn (wet seasons) and the occurrence of predominantly liquid precipitation at lower elevations and snow at the CKS1Karabatkak glacier in spring. Thus, in CKS catchment, *d*D-*excess* values for snow and rain were 9.7‰ and 15.3‰, respectively (Table S1). By contrast, in DJF, when the sub-cloud evaporation effect is absent (Fröhlich et al., 2001), *d*D-*excess* values declined with elevation between the CKS2Lesnoy Cordon and CKS3TSC sites. The domination of the Siberian high limits advection of moist air to the central Tien Shan in winter resulting in low precipitation across the region (Fig. 1). However, the CKS3TSC site is located in proximity to Lake Issyk Kul and it may be suggested that evaporation from the lake contributes to precipitation with more positive~~less depleted isotopic signatures while the suppression of convection results in a gradient between the two sites (Fig. 3c).

In CHK, ~~at the higher-elevation sites of CHK2Pskem (1255 m a.s.l.) and CHK1Oygaing (1490 m a.s.l.),~~ ~~*d*D~~-*excess* values changed little at the higher-elevation sites of CHK2 (1255 m a.s.l.) and CHK1 (1490 m a.s.l.) in DJF, MAM, and SON (between both, seasons and ~~between the~~ sites). The largest seasonal variations ~~differences~~ occurred at the low-elevation (486 m a.s.l.) ~~CHK3lower elevations but were inconsistent between seasons~~. The steepest elevational gradients were observed in ~~summer~~JJA when the ~~when the relationships between elevation and *d*D-*excess* were non-linear and seasonal~~mean seasonal ~~*d*D~~-*excess* ~~values~~ declined from 16.5‰ (n=2) in CHK3~~Tashkent~~ to a negative value of -3.9‰ (n=4) in CHK2. This trend was opposite ~~Pskem~~to CKS. ~~–~~Similar but less pronounced gradients were~~as~~ observed in SON. The high *d*D-*excess* values at CHK3~~Tashkent~~ were not consistent with its low elevation ~~(486 m a.s.l.)~~, high air temperature observed during the considered precipitation events (29.8°C) (Table S3), and ~~low amounts of~~ small precipitation depth (on average, 0.1 mm per event).

Analysis of the overall event-based data set showed that ~~T~~there were no significant geographical controls over *d*D-*excess*, ~~including latitude, longitude and elevation, were investigated using stepwise regression for all the event-based samples (Table 1). The following regression equation was obtained~~. However, analysis of the seasonal sub-sets showed that :

~~$D\text{-}excess = 51.9 - 1.29Lat + 0.16Lon + 0.002E$ (10)~~

~~Longitude~~ elevation~~Elevation~~ was a significant~~ly~~ ~~correlated~~predictor of *d-excess* ($p < 0.01$) ~~with *d*D-*excess* across the region and~~ in all seasons. ~~Elevation~~ Longitude was statistically significant predictor~~s~~ of *d-excess* in~~for~~ MAM ($p < 0.05$) and SON ($p < 0.05$) ~~DFJ, JJA, MAM ($p < 0.01$) and SON ($p < 0.05$) while latitudeongitude was not a significant predictor for *d-excess* in MAM ($p < 0.05$) and SON ($p < 0.05$)~~ (Table S2).

3.3 LMWL for ~~of~~ the mountains of Central Asia

LMWLs were calculated ~~firstly~~ using the whole data set and ~~then for each~~ for the individual catchments (Tables S5-9). The LMWL developed from the whole set of the event-based precipitation samples (Table 1; Fig. 4a) using the most common unweighted OLSR method (Section 2.3) was:

Formatted: Font:Italic

Formatted: Font:Italic

Formatted: Font:Italic

Formatted: Font:Italic

Formatted: Font:Italic

$$\delta D = (7.56 \pm 0.05)\delta^{18}O + (8.65 \pm 0.54),\ R^2 = 0.96 \quad (10)$$

The LMWL developed from 149 mean monthly values including the Dushanbe monthly cumulative precipitation samples (Fig. 4b) using the same regression method was:

$$\delta D = (7.6 \pm 0.1)\delta^{18}O + (9.6 \pm 1.2),\ R^2 = 0.97 \quad (11)$$

Figure 4 and Table S5 show the parameters of the derived regression equations. The slope and intercept values were lower (Equations 10-11; Fig. 4a-c) than those of the GMWL (Dansgaard, 1964). The 95% confidence intervals in Equation 10 were 7.6 − 9.7 for the intercept and for 7.5 − 7.7 for slope, respectively. the respective confidence intervals in the Equation 11 were 7.2 − 11.9 and 7.3 − 7.8. ~~Although, isotopic ratios are controlled by the equilibrium fractionation, in the arid regions, where significant evaporation of precipitation is observed especially during the events of light precipitation or virga, kinetic fractionation is important resulting in the difference the GMWL and LMWL slopes (Tian et al., 2007; Wang et al., 2018, 2019; Chen et al., 2021). Seasonal variations in slope and intercept values (Putman et al., 2019), and in particular their lower values observed in summer, reflect the effects of sub-cloud evaporation too (Fig. 4d).~~ For the total study area, the slope changeds from 6.1±0.1 in JJA to 8.1±0.1 in DJF and intercept 2.7±0.7 in JJA to 13.8±2.1 in DJF. The DJF slope and intercept values in OLRS LWML, derived from 17 event-based samples, were lower in CKS than in other catchments at 6.7±0.5 and −12.1±8.3, respectively (Fig. 4d). The slope value for DJF was close to that in JJA (in contrast to other catchments) indicating strong evaporation from the lake.

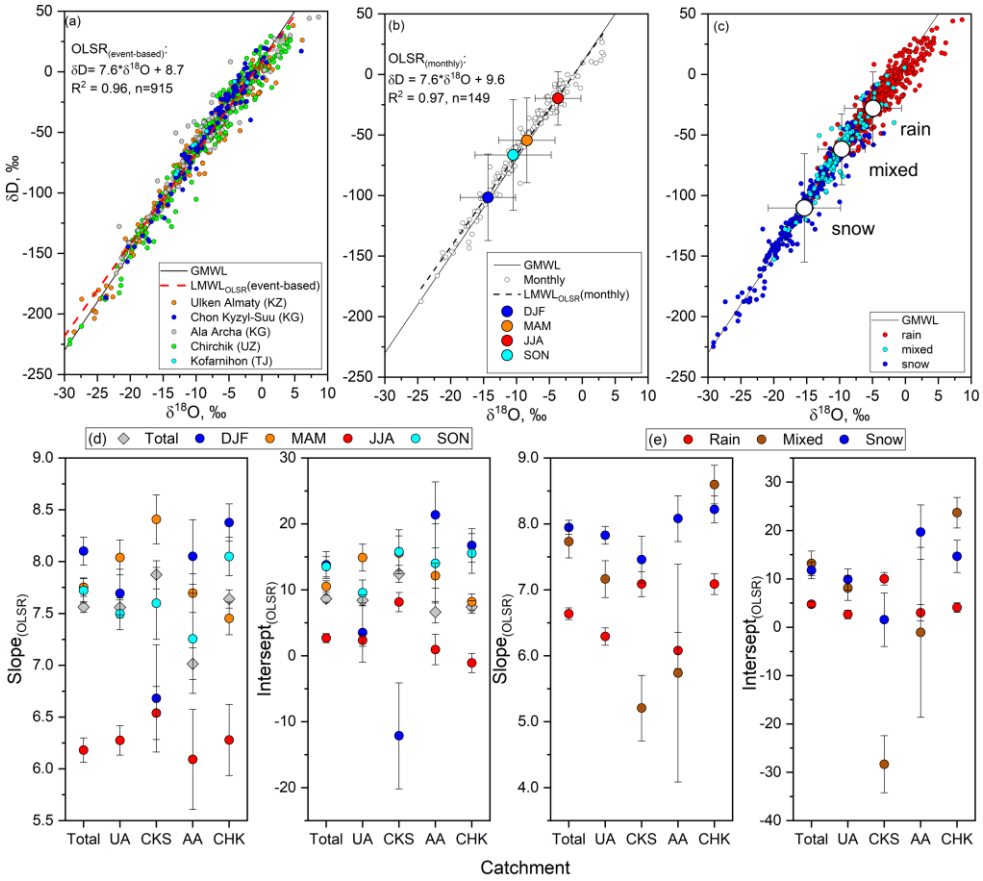

Figure 4: The upper panel shows dual δD and $\delta^{18}O$ plots for (a) the event-based samples for individual catchments, (b) monthly averaged values and seasonal means, and (c) different types of precipitation. The lower panel shows the OLSR-based LMWL slopes and intercepts using (d) event-based data for each catchment by season and (e) by type of precipitation.

~~The effect of Lake Issyk Kul (Fig. 1a; Section 3.2) was clearly visible in the CKS data for winter. The DJF slope and intercept values in OLRS LWML, derived from 17 event-based samples, were lower than in other catchments at 6.7±0.5 and −12.1±8.3, respectively (Fig. 4d). The slope value for DJF is close to that in JJA (in contrast to other catchments) indicating strong evaporation from the lake.~~

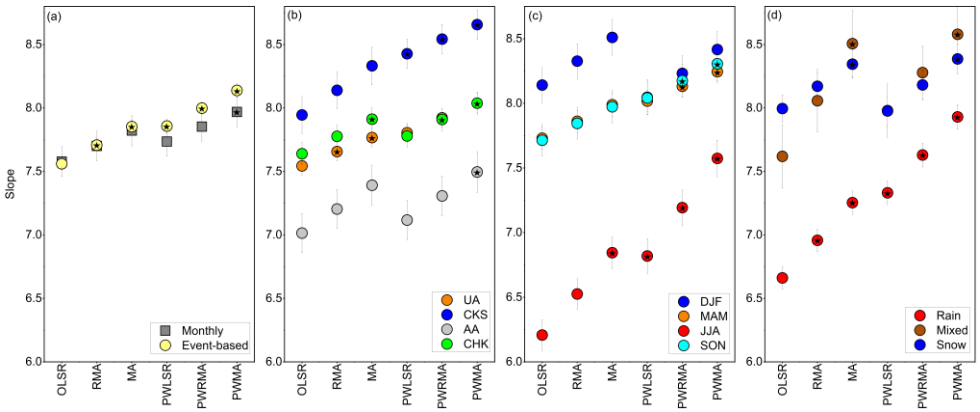

Figure 5: LMWL slopes derived from the regression equations developed using six methods (see Section 2.3 for abbreviations) for (a) event-based and monthly data set for all samples across the region, (b) by catchment, (c) by season, and (d) by precipitation type for the event-based samples. Statistically significant values are marked with a star sign. The values of slopes and intercepts and the outcomes of t-test of between-method differences are presented in Tables S5-S9.

The performance of different regression methods was assessed using the RMSSEav statistics (Section 2.3). For all six methods, RMSSEav values were close to 1 indicating good performance, however, the best regression fit was obtained by the RMA and PWLSR methods for the non-weighted and weighted precipitation, respectively (Table S6-S9). Generally, the weighted methods (PWLSR, PWRMA, and PWMA) generated steeper LMWL slopes than the non-weighted methods (OLSR, RMA, and MA). However, ~~a~~ t-test, applied to assess the differences between the regression metrics generated by the six methods and OLSR, showed that ~~the~~ results of the RMA method were not significantly different from OLSR ($p > 0.05$) when calculations were made for individual basins, seasons, and types of precipitation with two exceptions: (i) event-based rain only sub-set~~ample~~ and (ii) all event-based samples combined across the region (Tables S5, S9). Parameters of the regression equations for each catchment, season, and precipitation type are shown in Tables S5-S9. Here, the outcomes from the OLSR and PWLSR methods are summarised.

For the whole region, the slope~~s~~ values varied from 7.6 (monthly and event-based) OLSR to 7.7 (monthly) and 7.9 (event-based) using PWLSR (Fig. 5a). ~~This implies that both monthly and even-based samples can be used to develop LMWL for the region.~~ The performance of the methods varied between catchments (Fig. 5b). The largest between-method differences were observed in CKS (n=149) with slope values ranging between 7.9 (OLSR) and 8.4 (PWLSR). Statistically significant differences between the non-weighted OLSR and the weighted PWLSR method were observed in AA and CHK because of the lower amounts of precipitation, especially in CHK in summer. In the UA and CKS, the differences were not significant. The slope values derived from the event-based precipitation data for SON (n=138) and DJF (n=168) did not vary significantly between the OLSR and PWSLR methods (Fig. 5c) while ~~in MAM (n=273) and JJA (n=290)~~ they were significantly different in MAM (n=273) and JJA (n=290). Larger differences were observed in JJA (n=290) when~~re~~ slope values varied from 6.2 (OLSR) to 6.8 (PWLSR) (Fig. 6c). The similarly large differences characterised the rain sample sub-set (n=514) with slope values ranging from 6.7 (OLSR) to 7.3 (PWLSR) (Fig. 5d).

3.4 Relationships between isotopic composition and ~~moisture sources~~precipitation provenance

Overall, 766 five-day (120 hours) back trajectories were generated for every precipitation event for four sampling points: UA1~~BAL~~ (~~UA,~~ n=338), CKS2~~Lesnoy Cordon~~ (~~CKS,~~ n=117), AA1~~Baityk~~ (~~AA,~~ n=115), and CHK1~~Oygaing~~ (~~CHK,~~ n=196) (Table 1). Overall, five clusters were identified: northern part of Kazakhstan – southern Siberia (North - Cluster 1), south-eastern Europe, Black Sea and Caspian Sea (West - Cluster 2), Iran and eastern Mediterranean (South-West - Cluster 3), lower reaches of the Syr Darya and Amy Darya and irrigated area around the Aral Sea (Aral - Cluster 4), and precipitation formed within the study catchments (Local - Cluster 5).~~Although the mixing model was limited to a maximum of three contributing sources (Equations 4 – 5), the number of clusters derived for each site was not limited to three (to avoid discarding important circulation groups). Initially, the number of clusters was determined by plotting the distances between the merged clusters as a function of stage in the cluster analysis (Wilks, 1995).~~

~~For each site, between three and five clusters of back trajectories were identified and similar trajectory clusters from different sites were merged to form five trajectory groups (Section 2.4; Fig.6). Three criteria were used for merging the identified clusters into groups (i) direction of travel; (ii) distance travelled; (iii) whether local circulation trajectories remained within the catchment boundaries. Five synoptic groups included the northern part of Kazakhstan – southern Siberia (North - Group 1), south-eastern Europe, Black Sea and Caspian Sea (West - Group 2), Iran and eastern Mediterranean (South-West - Group 3), lower reaches of the Syr Darya and Amy Darya and irrigated area around the Aral Sea (Aral - Group 4), and precipitation formed within the study catchments (Local - Group 5).~~

Clusters~~Groups~~ 1 and 2 were identified at each site accounting for 6-26% and 5-19% of all trajectories (Table 2; Fig. 7). The ~~Group~~Cluster 1 trajectories were most frequent ~~in the~~at UA1 and least frequent ~~in the~~ at CHK1~~2~~ ~~catchments a~~and were the most frequent group in JJA overall. In DJF, the Cluster 1 trajectories were registered only one and eight times at UA1 and CHK2 (Fig. 7). The Cluster~~Group~~ 2 trajectories were most frequent ~~in the~~ at CHK1~~2~~, and least frequent ~~in the~~ at UA1 (observed three times per season in MAM, JJA and SON) and CKS2 (observed twice per season in DJF, JJA and SON ~~catchments~~). The ~~Group~~Cluster 3 trajectories ~~characterised moisture transport from~~ originated in Iran reaching ~~the~~ UA1 and AA1 ~~catchments~~ predominantly in DJF and MAM but they were not observed at CHK~~2~~1 and CKS2 (Fig. 7). ~~We note that, w~~While limiting trajectories to 120-hour duration places their origin in Iran, the extension of their duration leads to the eastern Mediterranean albeit with higher uncertainty ~~which increases with trajectory duration~~. Clusters~~Groups~~ 1, 2 and 3 represented the long-distance moisture transport with the mean trajectory lengths and standard deviations of 1738~~±~~451, 3285~~±~~1109 and 2652~~±~~185 km, respectively. Trajectories from Clusters~~Groups~~ 1, 2 and 3 represented ~~moisture transport~~ circulation along the peripheries of the low-pressure systems located north-west or west of the study region, and the differences between them were due to the latitudinal positions of the low-pressure system centres. Cluster~~Group~~ 4 included shorter trajectories (1188~~±~~237 km) to ~~the~~ UA1 and CKS2 ~~catchments~~ from the irrigated lands located along the Syr Darya and Amu Darya rivers, and the Aral Sea. This cluster~~group~~ accounted for 33% and 44% of all trajectories ~~to the~~ at UA1 and CKS2 ~~catchments~~, respectively (Table 2; Fig. 6), with the highest frequency in MAM and JJA (Fig. 7). The lengths of the 5-day trajectories in Cluster~~Group~~ 5, representing precipitation formed locally, varied between 292 km at CKS2 to 565 km at AA1 ~~catchments~~ with a mean length of 438~~±~~140 km. There is uncertainty about allocating ~~of~~ trajectories to Clusters~~Group~~ 4 and 5 ~~in~~at CHK1~~2~~ ~~catchment~~ because, although the ~~Group~~Cluster 5 trajectories satisfied the allocation criteria, the lower part of the CHK catchment is irrigated and the Chirchik is a tributary of the Amu Darya. Trajectories of this cluster~~group~~ were observed at each site accounting for 26% (UA1) to 45-61% (other sites) of all trajectories (Table 2).

Formatted: Not Highlight

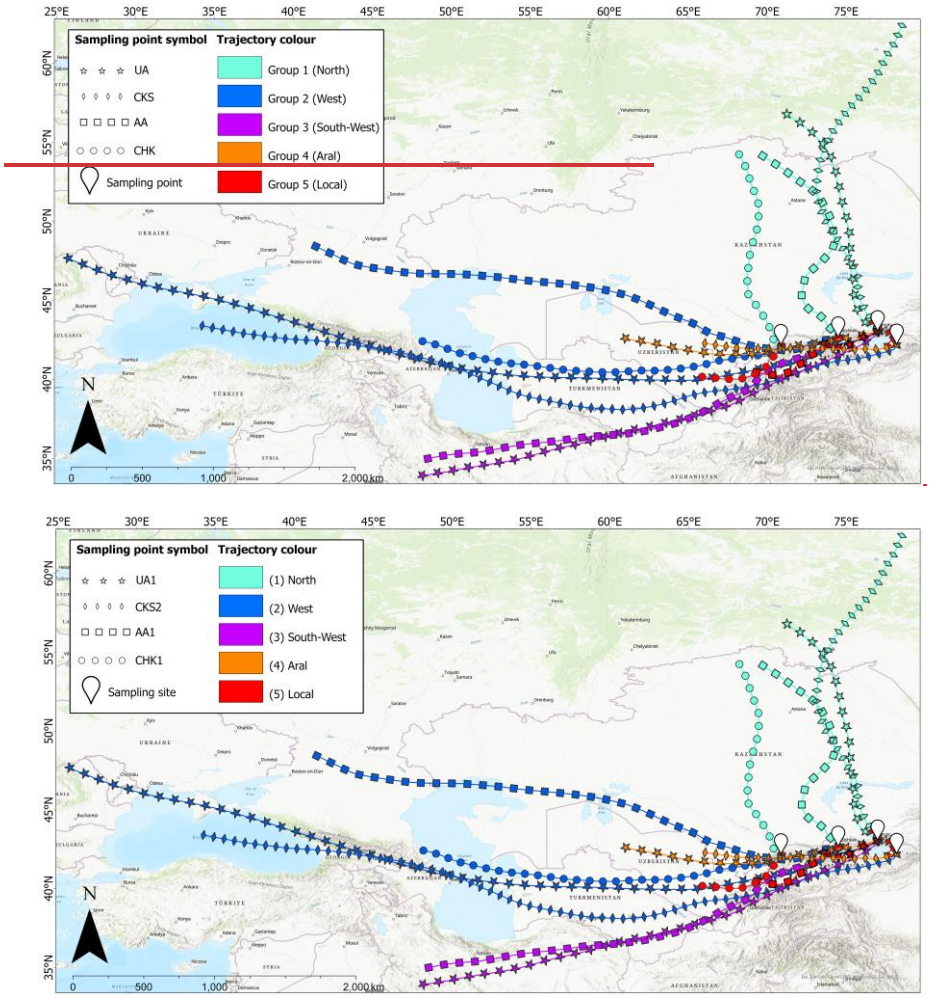

Figure 6: Trajectory ~~groups~~clusters including mean back trajectories (as generated by HYSPLIT) for the original clusters for four sampling sites for the study period. ESRI ~~ArcGis~~ArcGIS Pro ~~basemaps~~ Word Topographic Map and World Hillshade are used as background.

Isotopic ratios and *d*~~D~~ *excess* values averaged over the trajectory ~~groups~~clusters by site are shown in Table 2; the box plots are shown in Figures S2 and S3. ~~further illustrate variation of seasonal values of isotopic ratios and *d*D *excess* within each original cluster by site. Statistical significance of differences between the clusters and groups (Fig. 7; S2–3) were assessed using ANOVA.~~

The between-cluster~~group~~ differences in $\delta^{18}O$ were largest in JJA and DJF, while in MAM- and SON (wet seasons; Fig. 1c), they were not statistically significant at 95% confidence level (Fig. 7). In DJF, isotopic ratios of Cluster 1 precipitation ~~samples associated with Group 1~~ were ~~more~~ less negative ~~least depleted~~ with ~~the~~ the mean $\delta^{18}O$ value of -12.01‰ while ~~samples~~ ratios

Formatted: Font:Italic

associated with ~~Group~~Cluster 2, representing the most long-distance transport from the west, were ~~most~~more negative ~~depleted~~ with the mean $\delta^{18}O$ of -18.29‰ (Fig. 7a). However, the ~~the higher~~less negative values of ~~enrichment of~~ $\delta^{18}O$ and δD were~~as~~ observed at~~in~~ AA1 ~~for~~in ~~Group~~Cluster 2 (−6.4 ‰ and −35.0‰, respectively) whereby trajectories started over the East European Plain and crossed the ~~arid~~deserts of western ~~of~~ Kazakhstan. In JJA, the highest mean $\delta^{18}O$ values of 0.01‰ ~~were associated~~ characterised with ~~Group~~Cluster 2. T~~-trajectories while t~~he lowest mean $\delta^{18}O$ values ~~of −6.94‰~~ characterised Cluster~~Group~~ 3 in both JJA and SON (~~trajectories which also exhibited the lowest mean $\delta^{18}O$ value of~~ −6.94‰ and −~~-~~17.6‰, respectively). ~~-in SON,~~Cluster 5 was characterised by the highest in-cluster variability in $\delta^{18}O$. At UA1, AA1, and CHK2, Cluster 5 trajectories arrived predominantly from the south-west and corresponded to more negative isotopic values while at CKS2, they arrived from the north-east and corresponded to the higher isotopic ratios (Fig.6; Table 2).

The between-cluster differences in *d-excess* were significant in all seasons except SON (Fig. 7b). In DJF, the lowest mean *d-excess* value (5.7‰) characterised Cluster 2 and highest (18.6‰) – Cluster 1 (Fig. 7b). The highest mean JJA value of 17.2‰ characterised Cluster 3 arriving from Iran to UA1 and AA1. Cluster 4 trajectories originating over the irrigated lands in the Aral Sea basin had the mean annual *d-excess* of 14.4‰ and 13.9‰ at UA1 and CKS2 (Table 2). Cluster 5 was characterised by the highest variability in *d-excess* values (Fig. 7b).

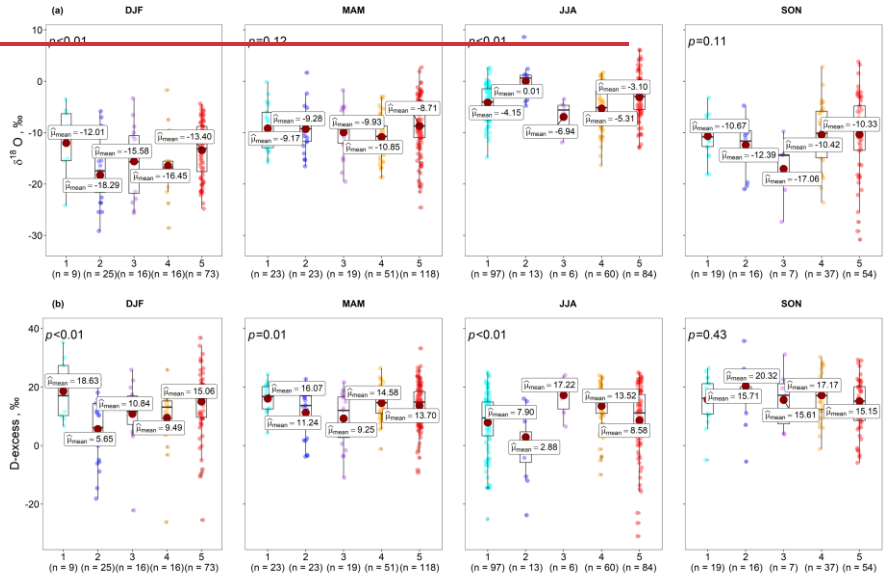

Formatted: Not Highlight

Formatted: Not Highlight

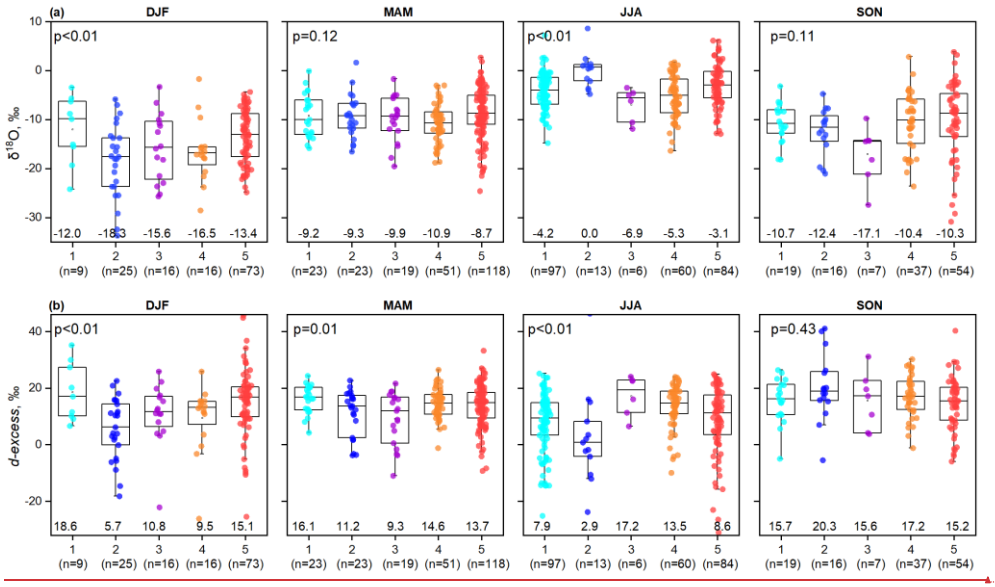

Figure 7: Seasonal values of (a) $\delta^{18}O$ and (b) *d*~~D~~-*excess* according to the trajectory ~~groups~~clusters. Numbers along the X-axes show the number of events in each group and season. ~~The figure was produced using the RStudio package ggstatsplot (Patil, 2021)~~

~~The between-group differences in *d*D-*excess* values were significantly different in all seasons except SON (Fig. 7b). In DJF, *d*D-*excess* showed the opposite pattern to $\delta^{18}O$ being lowest (5.65‰) in the samples associated with Group 2 westerly trajectories and highest (18.63‰) with Group 1 northerly trajectories (Fig. 7b). The former is associated with moisture from the Black Sea area characterized by higher relative humidity, and the latter can be associated with low relative humidity over Eurasia in winter (Bershaw, 2018; Kostrova et al., 2020). By contrast, in JJA, high humidity is observed over Siberia which decreases the evaporation diffusivity ratio resulting in lower *d*D-*excess* associated with Group 1 (Kostrova et al., 2020). The highest mean JJA value of 17.22‰ characterised the Group 3 trajectories arriving from Iran to the UA and AA catchments. Group 4 trajectories originating over the irrigated lands in the Aral Sea basin had the mean *d*D-*excess* of 14.4‰ and 13.9‰ in the UA and CKS catchments, respectively, indicating the contribution of re-evaporated moisture to precipitation. The largest proportion of precipitation events (which were also the heaviest) was associated with the Group 5 local trajectories (n=329), and precipitation formed in the local air masses upon orographic uplift (Table 2). Trajectories of this group accounted for 53% and 50% of all events in DJF and MAM. In JJA and SON, their share declined to 42% and 30% of all events, respectively, but they remained the most frequent group in SON and the second most frequent (after Group 1) in JJA. This group was characterised by the highest in-group variability in both trajectory direction, which veered strongly while the travelled distances remained short, and associated $\delta^{18}O$ and *d*D-*excess* values. In the UA, AA, and CHK catchments, Group 5 trajectories arrived predominantly from the south-west and corresponded to more depletednegative precipitation isotopic values while in CKS, they arrived from the north-east and corresponded to the higher isotopic ratios (Fig.6; Table 2). The mean *d*D-*excess* values remained high in SON, DJF and MAM ranging between 13.07‰ and 15.15‰ and indicating atmospheric conditions at the moisture source or the contribution of the re-evaporate moisture. In JJA, the mean *d*D-*excess* value was 8.58‰ (which is just below the global mean) and the median value was 11.2‰ while individual *d*D-*excess* values ranged between -31.0‰ and 25.0‰ (Fig. 7b). The standard deviations were high not only in JJA but also in DJF at ±11.98‰ in both seasons.~~

Formatted: English(United Kingdom)

Formatted: Font:Italic

Table 2: Frequency of trajectories by cluster~~group~~ and mean values (upper line) and standard deviation (lower line) of $\delta^{18}O$, δD and *d*~~D~~-*excess* (‰) ~~by sampling sites and trajectory clusters~~. C is cluster; SD is standard deviation; N is number of trajectories corresponding to individual precipitation events and their proportion of the total for each site; Lat is latitude (ºN), Lon is longitude (ºE); D is distance from ~~the moisture~~ trajectory source (120 hour iteration) to the sampling point (km). Seasonal mean temperature and total and mean precipitation were derived for the days when precipitation samples were collected over the sampling period (Table 1) and averaged (summed) over ~~a given~~ trajectory cluster~~s~~ and season~~s~~.

C	$\delta^{18}O$	δD	*d*~~D~~-*excess*	Lat	Lon	N (%)	D	Seasonal mean t, ºC				Seasonal mean P, mm/event				Seasonal total P, mm			
	Mean (upper line) / SD (lower line)							DJF	MAM	JJA	SON	DJF	MAM	JJA	SON	DJF	MAM	JJA	SON
								~~BAL (UA)~~UA1											
1	-6.9	-43.9	11.7	56.46	70.83	88	1625	-10.4	-2.1	7.3	-0.8	2.0	10.7	4.6	4.9	2	85	277	88
	4.4	31.2	8.6	6.41	9.27	(26)													
2	-15.9	-120.0	6.8	46.49	25.75	17	4452	-13	-6.1	10.8	2.1	4.4	5.8	2.3	6.0	35	17	5	6
	9.9	77.5	10.8	12	7.16	(5)													
3	-13.5	-98.1	10.1	33.59	48.51	31	2782	-10.2	0.0	5.6	-8	2.3	6.9	11.5	3.3	23	69	69	17
	7.1	56.0	10.8	5.93	8.78	(9)													
4	-9.8	-63.9	14.4	42.4	61.06	113	1355	-9.5	-0.2	7.3	-1.3	4.1	5.2	6.3	4.2	45	194	252	104
	6.1	46.2	6.9	5.48	6.48	(33)													
5	-8.5	-55.3	12.9	42.1	73.29	89	345	-9.6	-0.6	7.8	0.6	3.6	7.0	4.8	3.3	22	169	148	85
	6.6	48.5	10.4	2.57	6.86	(26)													
								~~Lesnoy Cordon (CKS)~~CKS2											
1	-7.7	-41.8	19.8	61.32	77.2	7	2403	-	0.6	9.1	-	-	5.2	14.1	-	-	16	56	-
	4.1	36.0	4.9	7.08	20.16	(6)													
2	-12.5	-83.8	16.2	44.68	31.4	6	3910	-4.2	-	10.4	-6.8	8.9	-	7.3	10.7	18	-	15	21
	7.7	62.0	3.5	6.33	25.5	(5)													
4	-8.1	-51.0	13.9	42.57	66.33	51	1020	-3.6	2.4	9.6	5.8	3.4	7.6	5.8	6.8	17	99	117	74
	5.5	46.7	9.1	4.71	6.68	(44)													
5	-6.3	-38.6	12.0	43.89	75.83	53	292	-	6.0	10.4	1.8	-	7.1	5.5	6.5	-	150	148	26
	4.9	37.0	10.0	3.21	3.72	(45)													
								~~Baityk (AA)~~AA1											
1	-5.2	-31.7	9.5	53.71	70.3	14	1497	-	2.4	17.4	3.9	-	7.2	3.8	5.4	-	43	27	5
	6.1	39.8	3.5	6.55	10.14	(12)													
2	-6.4	-35.0	15.9	47.09	41.76	17	2798	-5.7	-1.2	17.6	2.6	7.4	6.2	2.9	5.2	15	12	17	36
	6.8	44.8	4.6	7.67	18.62	(15)													
3	-10.6	-70.0	14.6	34.81	48.5	17	2521	-2.9	4.9	-	-2.4	2.9	4.3	-	10.0	17	39	-	20
	4.9	36.2	1.8	7.41	7.45	(15)													
5	-9.0	-56.2	15.8	40.18	68.91	67	565	-4.7	6.0	13.6	7.4	4.0	6.6	5.3	5.1	88	132	79	51
	6.7	49.9	1.4	3.21	5.52	(58)													
								~~Oygaing (CHK)~~CHK1											
1	-4.8	-30.7	7.7	54.33	68.29	39	1427	-4.1	0.9	13.2	-	4.5	2.7	5.7	-	36	16	143	-
	5.7	42.1	12.4	6.33	8.94	(20)													
2	-11.3	-82.5	7.5	42.02	48.01	37	1981	-8.3	2.1	15.1	0.0	4.9	5.6	6.2	6.4	59	100	12	32
	7.1	55.7	10.3	8.62	10.65	(19)													
5	-9.4	-63.5	11.8	40.03	65.98	120	549	-4.1	3.0	12.8	-3.4	5.8	6.6	2.3	4.0	263	347	23	48
	7.2	57.7	10.3	3.84	6.53	(61)													

3.5 Relative contributions of moisture sources to precipitation

~~The cluster analysis outcomes of the HYSPLIT back trajectories combined with the isotopic signatures were used to quantify the relative contributions of the identified moisture sources to precipitation in the study region and to calculate the proportion of recycled moisture using the three-component linear mixing model (Equations 4, 5 in Section 2.5). To reconcile the number of synoptic groups with the three-component models, Groups 1, 2, and 3 were merged (westerly group) because, despite the differences in directions, they were associated with the long-distance transport along the peripheries of depressions originating over the Atlantic (Section 3.3).~~ The three components of the mixing model (Equation 4) were~~:~~ (i) δ_A – precipitation formed inland over the Aral basin (Cluster~~Group~~ 4); (ii) δ_B – local ~~moisture~~ly-formed precipitation ~~-~~(Cluster~~Group~~ 5); and (iii) δ_C – precipitation associated with the Atlantic depressions (merged Clusters~~Groups~~ 1 – ~~-~~3) and δ_P was the mean seasonal value of the isotopic ratios (Fig. 8). Using ~~the~~ UA1 ~~catchment~~ in DJF as an example, the mean seasonal precipitation isotopic ratios (δ_P) were~~are~~ −134.5 ‰ for δD and −~~-~~17.9 ‰ for $\delta^{18}O$, respectively. The three components of mixing model isotopic ratios were: δ_A (−121.6 ‰ for δD and −~~-~~17.1 ‰ for $\delta^{18}O$), δ_B (−91.9 ‰ for δD and −~~-~~12.7 ‰ for $\delta^{18}O$), and δ_C (−154.3 ‰ for δD and −~~-~~19.9 ‰ for $\delta^{18}O$). ~~In the~~At UA1, three groups of trajectories ~~representing three moisture sources~~ were ~~represented~~ registered in each season and ~~in~~ at CKS2 – in all seasons except DJF when there was no precipitation associated with~~no~~ local trajectories ~~were observed~~. Only two groups – ~~(sources)~~ – local ~~recycled moisture~~ and the westerlies – ~~-~~ were represented ~~in the~~at AA1 and CHK2 ~~catchments~~.

The proportional contributions of the identified trajectory sources at different sites and seasons are shown in Table 3. The westerly flow was the main contributor to precipitation at UA1 in winter (54%) and at UA1 and CHK2 in summer (49% and 73%, respectively). The Aral basin contributed 46% at UA1 in MAM, and 71.2% and 67.3% at CKS2 in DJF and SON, respectively. In other seasons, the contribution from Aral basin varied between 29% and 37%. Contributions of the locally formed precipitation ranged from 16% to 73% being particularly high at CKS2 in MAM and JJA while the absence of contribution local sources in DJF was likely an artifact of the small number of samples (n=7). Locally formed precipitation prevailed throughout the year at AA1 and at CHK2, except JJA.

Formatted: Not Highlight

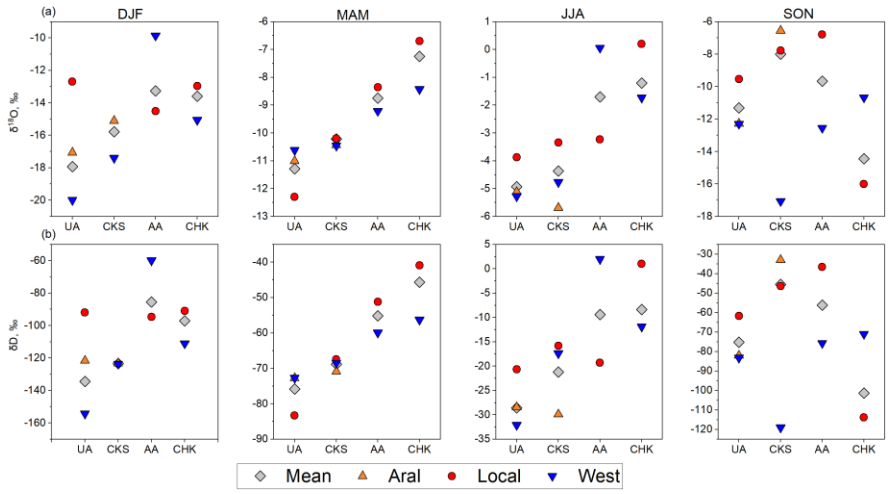

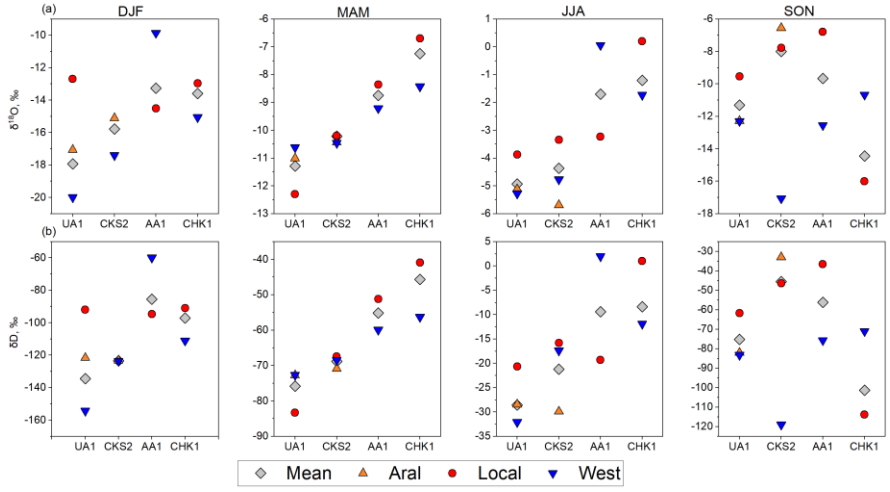

Figure 8: The values of $\delta^{18}O$ (a) and δD (b) characterising seasonal precipitation (δ_P), precipitation originating over the Aral basin (δ_A), locally formed precipitation (δ_B), and precipitation associated with the westerly transport (δ_C) for each basin.

Table 3: Proportional contributions of moisture sources (%) to precipitation and standard errors (SE).

Catchment	Aral				Local				Westerly			
	DJF	MAM	JJA	SON	DJF	MAM	JJA	SON	DJF	MAM	JJA	SON
	Mean (upper line) / SE (lower line)											
UA1	29.1	45.7	29.6	29.5	16.5	29.3	21.6	36.0	54.3	25.0	48.8	34.5
	2.0	3.1	2.1	10.7	1.0	0.6	0.6	0.4	1.0	2.7	1.7	10.4
CKS2	71.2	36.5	37.0	67.3	-	54.3	51.8	21.5	28.8	9.2	11.2	11.2
	1.6	3.4	0.4	5.1		1.9	0.6	5.9	1.6	4.2	0.9	0.8
AA1	-	-	-	-	73.3	54.1	53.6	50.1	26.7	45.9	46.4	49.9
					0.3	1.4	0.4	0.3	0.3	1.4	0.4	0.3
CHK1	-	-	-	-	69.5	68.8	26.9	70.6	30.5	31.2	73.1	29.4
					0.5	0.4	0.4	0.6	0.5	0.4	0.4	0.6

4 Discussion

4.1 ~~Filling the gap in the global database of isotopic ratios and assessing r~~Regional trends in isotopic ratios and ~~d~~ *excess*

Clear seasonal cycles of $\delta^{18}O$ and δD were observed in every catchment with higher $\delta^{18}O$ and δD values registered in summer and lower in winter (Fig. 2) in line with the annual temperature cycle (Fig. 1 b). The maximum enrichment occurred between

Formatted: English(United Kingdom)

Formatted: English(United Kingdom)

Formatted: English(United Kingdom)

Formatted: English(United Kingdom)

Formatted: Font:Italic

June in the south (e.g. CHK) and in July–August further north while the most negative values were registered between November and February (Fig. 2; Table S1). In the CKS catchment, the lake effect was evident in the cold season due to the contrast between an enhanced contribution of heavier water vapour from the lake and lighter vapour delivered by the cold air masses (Bowen et al., 2012; Xiao et al., 2017; Minder et al., 2020) resulting in the less negative isotopic ratios of precipitation (Fig. 2). Air temperature was a statistically significant predictor of $\delta^{18}O$ and δD but coefficients of determination of 0.46 – 0.66 implied that using air temperature as proxy for isotopic signatures may lead to high uncertainty in the reconstructions of isoscapes in the mountains~~topolgues~~. Similar coefficients were obtained for the Chinese Tien Shan (Wang et al., 2017, 2022), northern Kazakhstan (Yapiyev et al., 2020), and other high- and mid-latitude regions (Gat and Gonfiantini, 1981; Gat, 1996; Rozanski et al., 2013; Putman et al., 2019) although stronger links were reported by Kostrova et al. (2020) for south-eastern Siberia. The $\delta^{18}O$ and δD values changed by 0.62‰ and 4.68‰ per one degree Centigrade, respectively, for the whole data set which is consistent with the results for the Upper Urumchi basin in the Chinese Tien Shan (Pang et al., 2011). Temporal variability in isotopic ratios was stronger in winter and this was also confirmed by the comparison of the snow and rain data sets (Table S1 and Fig. 4). In winter, day-to-day temperature fluctuations, associated with changing synoptic conditions, are stronger than in summer with mean temperature changes between two consecutive days of 4ºC (Shahgedanova, 2002). There was no statistically significant link between isotopic ratios and event precipitation depth even in the arid CHK catchment. Previous studies conducted in the neighbouring regions (Liu et al. 2014; Wang et al., 2018; Juhlke et al., 2019) and globally (Bowen, 2010; Bowen et al., 2019; Putman et al., 2019) also concluded that this correlation was weak.

The observed seasonal cycles of $\delta^{18}O$ and δD were generally consistent with the global interpolation of precipitation isoscapes (Bowen and Revenaugh, 2003; Bowen et al., 2019), the global high-resolution isotope precipitation data (Terzer-Wassmuth et al., 2021), and results reported for the Chinese Tien Shan (Liu et al., 2014; Wang et al., 2019). However, the interpolations significantly underestimated isotopic ratios in the study region between October and March (Fig. 2 a, b) due to the lack of data available to date. For example, the annual mean difference between measured ratios and those derived from the global database (Fig. 2) varied from –0.3‰ (CHK) to 4.8‰ (CKS) for $\delta^{18}O$ and from −6.7‰ (CHK) to 37.4 (CKS) for δD but reached 10.1‰ (CKS) for $\delta^{18}O$ and 52.5‰ (AA) for δD in winter (Fig.2a, b; S1).

In CA, s~~An important achievement of this study is the development of an extensive database of isotopic ratios of precipitation and D-excess for the mountains of CA which enabled analysis of geographical, altitudinal, and temporal patterns in isotopic composition of precipitation and attribution of precipitation to regional sources. To date, very few measurements were available outside the Chinese sector of the Tien Shan. Contributing these data to GNIP (IAEA/WMO, 2015) will improve the representation of the CA mountains in the global high-resolution precipitation isoscapes database (Bowen and Revenaugh, 2003; Bowen et al., 2019; Terzer-Wassmuth et al., 2021), especially in the cold season when the differences between modelled (Bowen, 2022) and measured ratios were highest (Fig. 2). The advantages of the developed dataset are: (i) a wide geographical coverage from the northern Tien Shan (UA catchment) to the Gissar-Alay foothills (Dushanbe) (Fig. 1); (ii) sampling at different elevations within two catchments because of the limited availability of such data globally (Pang et al., 2011; Natali et al, 2022); and (iii) availability of the event-based precipitation samples enabling quantification of source region contributions to CA precipitation. The measurements complied with the IAEA quality standards as confirmed by the analysis of the test samples supplied by the IAEA (Wassenaar et al., 2021) assuring the quality of the isotope measurements performed in this study. The s~~patial variability in $\delta^{18}O$ and δD in precipitation in all seasons except autumn wa~~is characterised by an overall increase in isotopic ratios from north (UA)~~, where precipitation is more negative~~~~depleted~~, to south (CHK) (Table S1). The application of stepwise regression to the event-based data (Equations 6 – 7) showed that latitude was a statistically significant predictor of $\delta^{18}O$ and δD in the overall CA dataset. In the Chinese Tien Shan, mean isotopic ratios, measured at the mountain sites (between 1628 and 2458 m a.s.l. which is similar to the elevations of our sites), were less negative in the south-west and more negative in the north-east in JJA (~~This is different from the spatial trends reported by~~ Wang et al., (2016b). When

Formatted: Font colour: Auto

Formatted: Font colour: Auto

Formatted: Font colour: Auto

combined, both data sets confirm this spatial trend with mean JJA $\delta^{18}O$ changing from −1.2‰ and −1.7‰ in CHK1 (70.64°E) and AA1 (74.50°E) to −10.1‰ (93.03°E) and −10.5‰ (94.42°E) in China. In CA, elevation was a significant predictor of $\delta^{18}O$ and δD in winter and autumn and longitude − in autumn and spring, when westerly flow dominates. In the Chinese Tien Shan, there was no clear spatial or elevational trend at the mountain sites in DJF (Wang et al., 2016b). The number of sites in our study was relatively small (Table 1) and CKS experienced the lake effects. Both factors limited the performance of the regression model. Liu et al. (2014) used 29 sampling points in a similar analysis in northern China; Wang et al. (2016b) used 23 sites (although only six were in the mountains). ~~and Zhang and Wang (2018) for the Chinese Tien Shan where in winter, precipitation is more positive less depleted in the western and northern regions and more negative depleted in the inner and eastern sectors while in summer, there are no clear spatial trends. Winter precipitation is more depleted negative ($\delta^{18}O$ below −30‰) in the mountains and along the southern slope of the Chinese Tien Shan (Feng et al., 2013; Wang et al., 2016b) than in our study area possibly because a number of the Chinese sites are located in the isotopic rain shadow while sites used in this study are located on the upwind slopes (UA, CHK) or near a large lake (CKS). Isotopic ratios of winter precipitation measured over the Tibetan Plateau are closer to the values obtained in our study area than those obtained for the Chinese Tien Shan while summer precipitation appears to be more depleted negative in Tibet where summer temperatures are lower (Liu et al., 2014; Sun et al., 2019).~~

~~The application of stepwise regression (Equations 6–7) showed that latitude is a statistically significant predictor of $\delta^{18}O$ and δD in the overall dataset. Elevation and spring, and longitude are significant predictors in autumn and winter when westerly flow dominates, while latitude was single predictor for summer and the data from Wang et al. (2016b) also support this conclusion. Although we used the data from all sampling sites (Table 1), we note that the number of sampling sites was relatively small and sites in the CKS catchment were affected by Lake Issyk Kul. Both factors limit the performance of the regression model. For comparison, Liu et al. (2014) used 29 sampling points in a similar analysis in northern China.~~ The regression model can be improved in the future using isotopic data from a wider range of geographical locations, e.g. by combining ~~the~~ data sets from ~~the~~ CA and the Chinese ~~sectors of the~~ Tien Shan and by including the newly-established sites in the western Pamir where sampling commenced in 2023.

~~significantly influence of altitude and latitude while in DJF it mostly influenced by longitude than latitude. xxxxxxx.~~

~~A clear seasonal cycle in the isotopic ratios is observed in every catchment with less depleted negative precipitation registered in summer and more depleted negative in winter corresponding to the annual temperature cycle (Fig. 2). This is consistent with previous global studies (Bowen et al., 2019; Terzer-Wassmuth et al., 2021) and results reported for the Chinese Tien Shan (Liu et al., 2014; Wang et al., 2019). There was a strong positive correlation between the precipitation event-based isotopic ratios and air temperature with coefficients of determination of 0.46 – 0.66 (except Tashkent) similarly to the Chinese Tien Shan (Wang et al., 2017, 2022), northern Kazakhstan (Yapiyev et al., 2020), and other high- and mid-latitude regions (Gat and Gonfiantini, 1981; Gat, 1996; Rozanski et al., 2013; Putman et al., 2019). The $\delta^{18}O$ and δD changed by 0.62‰ and 4.68‰ per one degree Centigrade, respectively, for the whole data set which is consistent with the results for the Upper Urumchi basin in the Chinese Tien Shan (Pang et al., 2011).~~ Previous studies in the Chinese Tien Shan and in the western Pamir showed that the annual cycle of *d-excess* was opposite to those of $\delta^{18}O$ and δD with high (positive) values in the cold season and low (negative) values in summer (Pang et al., 2011; Wang et al., 2016b; Zhang and Wang, 2018; Juhlke et al., 2019). The JJA *d-excess* values in AA and CHK, calculated using unweighted precipitation, confirmed this conclusion being as low as –3.5‰ and similar to *d-excess* values measured in Iran and Iraq (Juhlke et al., 2019). Low precipitation amounts and higher temperatures, especially at CHK, enhanced negative *d-excess* values in JJA. There was a clear distinction between the AA and CHK catchments located in the west (72–74.5°E; Table 1) which matched the wider regional pattern, and CKS (78°E) located

Formatted: Superscript
Formatted: Superscript
Formatted: Not Highlight
Formatted: Not Highlight

in proximity to Lake Issyk Kul (Fig. 2c; Table S1) where the lake effect resulted in lower *d-excess* values which fell below 10‰ between January and April increasing to 20-22‰ in August-September (Fig. 2c). The annual *d-excess* cycle in the UA in the north-east of the study area (43°N; 77°E) was less pronounced. This sampling site was located by a much smaller (~ 0.8 km^2) mountain lake which freezes in winter. While locations of sampling sites were to an extent defined by the practical aspects of long-term monitoring, the presence of lakes complicated analysis of geographical *d-excess* patterns.

The observed elevational profiles of *d-excess* were inconsistent between sites and seasons (Fig. 3) partly because precipitation events were not always observed on the same days at different sites in the same catchment but also because of the different local conditions. At CKS, *d-excess* increased with elevation in summer in line with the decreasing air temperature and the distance that rain drops travel between the cloud base and land surface (Natali et al., 2022). This is consistent with a broader pattern of elevational change is d-excess described by Bershow (2018). In DJF, when the sub-cloud evaporation effect is absent (Fröhlich et al., 2001), *d-excess* values declined with elevation between the CKS2 and CKS3 sites. Lapse rates of *d-excess* were small in spring and autumn (wet seasons) likely due to the reduced sub-cloud evaporation and the occurrence of predominantly liquid precipitation at lower elevations and snow at CKS1 in spring. Thus, in CKS, *d-excess* values for snow and rain were 9.7‰ and 15.3‰, respectively (Table S1).

In CHK, low-intensity precipitation events dominated in JJA with 86% and 74% precipitation events producing less than 10 mm and 5 mm, respectively. At the same time, air temperatures were high even in the middle mountains, where most samples were collected (Fig. 1; Table 1), leading to a strong sub-cloud evaporation effect. The lowest mean *d-excess* value of –3.9‰ was registered at CHK2 (1255 m a.s.l.) in JJA increasing to an average of 1.3‰ at CHK1 (1490 m a.s.l.), similar to CKS (Fig. 3). However, the mean summer *d-excess* value of 16.5‰ in CHK3 (city of Tashkent, 486 m a.s.l.; derived from two precipitation events only) was inconsistent with the observed meteorological conditions. We suggest that Tashkent, located in the extensively irrigated foothills and featuring urban irrigation, may exhibit higher *d-excess* values in JJA (as well as SON) due to the contribution of water re-evaporated from the irrigated land. Similar oasis effects were reported by Wang et al. (2016a; 2016b) and Zhang and Wang (2018), however, a larger number of samples is required for confirmation.

~~Previous studies in the Chinese Tien Shan and in the western Pamir showed that the annual cycle of dD-excess was opposite to those of $\delta^{18}O$ and δD with high values in the cold season and low values in summer (Pang et al., 2011; Wang et al., 2016b; Zhang and Wang, 2018; Juhlke et al., 2019). In our study area, there was a clear distinction between the AA and CHK catchments located in the west of the study area (72-74.5°E; Table 1) which matched the wider regional pattern, and CKS (78°E) (Fig. 2c; Table S1). The annual dD-excess cycle in the UA catchment in the north-east of the study area (43°N; 77°E) was less pronounced. The distinguishing characteristic of CKS is its proximity to Lake Issyk Kul which does not freeze in winter. The UA sampling site was located by a much smaller (~ 0.8 km²) mountain lake which freezes in winter. While locations of sampling sites were to an extent defined by the practical aspects of long-term monitoring, the presence of lakes complicates analysis of geographical patterns of dD-excess patterns. The summer dD-excess values in AA and CHK, calculated using unweighted precipitation, were as low as -3.5‰ and similar to dD-excess values measured in Iran and Iraq (Juhlke et al., 2019). In CHK, low-intensity precipitation events dominated with 86% and 74% precipitation events producing less than 10 mm and 5 mm, respectively, in summer. At the same time, air temperatures were high even in the middle mountains, where most samples were collected (Fig. 1; Table 1), leading to a strong sub-cloud evaporation effect. Sampling was conducted at three elevations in CHK (Fig. 3). In summer, the lowest mean dD-excess value of -3.9‰ was registered at CHK2Pskem site (1255 m a.s.l.) increasing to an average of 1.3‰ at CHK1Oygaing (1490 m a.s.l.) corresponding to decreasing air temperature and the distance that rain drops travel between the cloud base and land surface (Natali et al., 2022). for confirmation.~~

~~As expected, the isotopic composition of solid and mixed precipitation was highly variable at each site (Table S1) due to the fractionation effect, while rainfall was characterised by the more consistent values (Fig. 4). This variability is a source of uncertainty in modelling cold season isotopic ratios (Fig. 2) (Bowen, 2022). There was no statistically significant correlation between isotopic ratios and event precipitation depth even in the arid CHK catchment. Previous~~

Formatted: Font:(Default)Times New Roman, Not Highlight

Formatted: Not Highlight

Formatted: Font:(Default)Times New Roman, Not Highlight

Formatted: Not Highlight

Formatted: Font:(Default)Times New Roman, Not Highlight

Formatted: Not Highlight

Formatted: Font:(Default)Times New Roman, Not Highlight

Formatted: Font:Italic

~~studies conducted in the neighbouring regions (Wang et al., 2018; Juhlk et al., 2019) and globally (Bowen, 2010; Bowen et al., 2019; Putman et al., 2019) also concluded that this correlation was weak. Positive values of the difference between isotopic ratios of $\delta^{18}O$ averaged over warm (May-October) and cold (November-April) periods, derived from the application of Dansgaard (1964) method, were similar to those obtained by Liu et al. (2014) for northern China where seasonal variations of air temperature of approximately 30°C were similar to the study region, and confirmed that the temperature effect dominated over that of precipitation depth.~~

~~4.2.~~ LMWL

LMWLs were developed for the study area for the first time to complement those for the Chinese sector of the Tien Shan (Wang et al., 2018). Although, isotopic ratios are controlled by the equilibrium fractionation, in the arid regions, where significant evaporation of precipitation is observed, especially during the events of light precipitation or virga, kinetic fractionation is important ~~,~~ resulting in the difference between the GMWL and LMWL ~~slopes~~ (Tian et al., 2007; Wang et al., 2018, 2019; Chen et al., 2021). ~~Seasonal variations in slope and intercept values (Putman et al., 2019), and in particular their lower values observed in summer, reflect the effects of sub-cloud evaporation too (Fig. 4d).~~

In CA, t~~T~~he availability of the LMWLs ~~is particularly important in CA because it~~ enables quantification of the relative ~~source~~ contributions of water sources, including precipitation, to runoff (Bowen et al., 2018; He et al., 2019) and calculation of ~~a~~ lake mass balance ~~using isotopes~~ (Yapiyev et al., 2020). Both tasks are relevant to adaptation policies in this water-deficient region.

Results obtained using monthly and even-based samples were close indicating that either can be used to develop LMWL in the region.

Application of the standard OLSR method to the data from individual catchments and seasons showed that higher slope values were observed in winter and spring (7.6 – 8.4) when the air temperature is lower and relative humidity is higher, and when precipitation peaks in spring. The lowest values (6.1 – 6.3) were observed in summer suggesting strong evaporation and a contribution to precipitation from local recycled moisture (Fig. 4; Table S5). The CKS catchment featured strong seasonal variations with the lowest slope value of 6.6 in DJF, pointing at evaporation from the Issyk Kul, and the highest value of 8.4 in spring. The seasonal variations in LMWL slope were consistent with those in the Chinese Tien Shan (Wang et al., 2018), however it is difficult to compare spatial variations in the LMWL slopes because of a limited number of sites used in this study. A clear north to south gradient in LMWL slope ~~is evident~~ was reported ~~based on studies in~~ for the Chinese Tien Shan and adjacent regions with the lowest values observed in the extremely arid Tarim basin (Wang et al., 2018). In our study region, the lowest summer and annual values were ~~are~~ observed in AA rather than in CHK catchment although AA is located in the northern part of the study area albeit in the inner Tien Shan.

Previous studies (Hughes and Crowford, 2012; Liu et al., 2014; Wang et al., 2018) demonstrated that low summer precipitation contributes to uncertainty in modelling LMWL. ~~For this reason, three derivations of the LMWL are available for GNIP stations by using OLSR, RMA and PWLSR.~~ Whilst there was no ~~t a~~ statistically significant ~~correlation~~ link between isotopic ratios and precipitation depth overall, the potential effects of low-intensity precipitation on summer isotopic ratios ~~and~~ especially in the more arid regions warrantied a comparison of ~~six~~ different LMWL derivation methods. ~~These covered~~ using non-weighted and weighted precipitation ~~and were applied to the region as a whole and to the individual catchments by season (Fig. 5; Tables S6, S7). The differences in the LMWL derived from T~~the methods using non-weighted precipitation ~~were small and~~ generated similar results which were not significantly different from the OLSR although the best fit was obtained ~~by~~ using RMA method (Table S6-9). The difference between methods based on weighted and non-weighted precipitation were small in all seasons

Formatted: Font:Bold, Font colour:Auto
Formatted: Space Before: 0 pt, After: 8 pt, Line spacing: 1.5 lines
Formatted: Not Highlight
Formatted: Not Highlight
Formatted: Not Highlight
Formatted: Not Highlight
Formatted: Not Highlight
Formatted: Not Highlight
Formatted: Not Highlight

except summer when the largest difference ~~between methods~~ was observed in (i) the AA and CHK catchments and ~~in~~(ii) the rain-only sub-set in all catchments (Fig. 5). The best fit was obtained using PWLSR method (Table S6-9).

In the Chinese Tien Shan, similar differences between methods based on weighted and non-weighted precipitation were observed ~~between~~ in the southern Tarim basin and the northern Junggar region (Wang et al., 2018). ~~However, AA is in the northern part of our study area albeit in the inner Tien Shan.~~ We~~,~~ ~~therefore,~~ recommend that the OLSR and RMA methods can be used in the mountains of CA except for the warm season when low rainfall depths are observed under high temperatures when the weighted precipitation the PWLSR method should be used.

4.3~~.~~ Trajectory sources and *d-excess*

Synoptic-scale patterns of *d-excess* are used to characterise changes in moisture sources but their interpretation is ambiguous especially in CA where water vapour travel large distances (e.g. Cluster 1-3) and is affected by secondary fractionation processes (Bershaw, 2018). In this study, ~~weighted precipitation and PWLSR method are used to develop LMWL during the warm season when low amounts of rainfall are observed under high temperatures in CA except in catchments located in the northern outer ranges of the Tien Shan such as the UA catchment in the Ile Alatau and the Junggar region in the Chinese Tien Shan.~~ there were well-pronounced differences between the mean *d-excess* values associated with different trajectory sources in all seasons except SON. The highest *d-excess* values in JJA (17.2 ‰; Fig. 7b) were predictably associated with trajectories arriving from Iran extending to the Mediterranean (if the iteration time exceeded 120 hours) in line with the uniquely high *d-excess* values characterising this region (Bershaw, 2018). Trajectories arriving from the Black Sea were by contrast characterised by the lowest mean *d-excess* values in both JJA and DJF (Fig. 7b) because the Black Sea region is characterized by high relative humidity throughout the year. Mean values of *d-excess* associated with Siberian trajectories cluster varied strongly between the highest in the data set in DJF (~~X~~18.6±10.3 ‰) and lower values in JJA (7.9±10.6~~X~~ ‰) in line with seasonal changes in ~~relative~~ temperature and humidity ~~highto relative lowsuppresses~~(Bershaw, 2018; Kostrova et al., 2020). Trajectories originating over the irrigated Aral Sea basin had the mean annual *d-excess* of 14.3±7.6~~XX~~‰ remaining consistently high throughout the year and indicating the contribution of re-evaporated moisture to precipitation.

4.43~~.~~ ~~Provenance 3 Main source regions of p~~Precipitation provenance in Central Asia

~~In previous studies, isotopic composition of precipitation and D-excess were used to trace source regions of moisture either using the isotopic signatures directly (Bershaw, 2018) or in combination with atmospheric trajectories (Crawford et al., 2013; Wang et al., 2017; Zhang and Wang, 2018; Juhlke et al., 2019). There are limitations to the former approach in CA because of its position in continental interiors away from the original marine sources of moisture, while the latter enables assessment of synoptic controls over the isotopic composition of precipitation. In this study, we used atmospheric back trajectories to examine atmospheric circulation controls using isotopic ratios and dD-excess.~~

~~We experimented with trajectories of different duration finally limiting it to 120 hours to minimise uncertainty in HYSPLIT modelling which increases strongly after this period of time (Draxler and Rolph, 2013). The mean water vapour residence time in the atmosphere is estimated by many studies as 8 - 10 days although its global median value was estimated as approximately five days (Van Der Ent and Tuinenburg, 2017). Therefore, limiting the length of back trajectories to 120 hours is not an issue for the shorter local and Aral Sea region trajectories. However, the identification of source regions in the westerly group (1-3) could be potentially affected especially in winter when water vapour residence time increases over the continental interiors in the Northern Hemisphere compared to summer (Van Der Ent and Tuinenburg, 2017).~~

Formatted: Not Highlight
Formatted: Font:Italic
Formatted: Heading2, Left, Space After: 8 pt
Formatted: English(United Kingdom)
Formatted: Font:(Default) Times New Roman, English (United Kingdom)
Formatted: Font:(Default) Times New Roman, Italic, English(United Kingdom)
Formatted: Font:(Default) Times New Roman, English (United Kingdom)
Formatted: Font:(Default) Times New Roman, English (United Kingdom)
Formatted: Font:Italic
Formatted: Font:Italic
Formatted: Font:Italic
Formatted: Font:Italic
Formatted: Not Highlight
Formatted: Not Highlight
Formatted: Not Highlight
Formatted: Affiliation
Formatted: English(United Kingdom)
Formatted: Space Before: 0 pt, After: 8 pt, Line spacing: 1.5 lines

The westerly airflow transporting the Atlantic moisture ~~to the study region wa~~is widely acknowledged as the main source of precipitation in CA based on studies of both climate (e.g. Shahgedanova, 2002) and isotope hydrology (e.g. Tian et al., 2007; Feng et al., 2013). ~~Our analysis showed that t~~This pathway was detected in all seasons, however, ~~the analysis also showed that the contribution of local recycled moisture is substantial. The~~ the mixing model results (Table 3; Fig. 8) showed that inland recycled moisture, originating from both the ~~vast~~ irrigated land in the Aral Sea region and from the study catchments, was~~is~~ the predominant source of precipitation in the study area. This conclusion agrees with Link et al. (2020) who showed that in Kyrgyzstan, the fraction of precipitation that originated from terrestrial sources reaches 61% making it one of the top 10 countries with the highest contributions from local terrestrial sources. Precipitation maxima in all catchments occur in MAM except UA where it peaks in May-July (Fig. 1). In MAM, precipitation associated with the local trajectories accounted for 52-54% in CKS and AA increasing to 69% in CHK. The Aral Sea region contributed 46% and 37% in UA and CKS, respectively (Table 3). Precipitation associated with the local within-catchment trajectories made the largest contribution at CHK (70%) and AA (73%), respectively. We attributed the high contribution of local sources to continuing evapotranspiration on the plains of Uzbekistan where temperatures remain mostly positive in winter. There was uncertainty about the separation of the locally formed precipitation from that forming over the Aral basin in CHK because the catchment is a part of the Aral basin with extensive irrigation. The westerly group made the largest contribution in UA, located on the northernmost slope of the Tien Shan, in JJA (49%) and DJF (54%) and in AA in all seasons (46-50%) except DJF.

The combined back trajectory and mixing model analysis has several limitations. Firstly, the performance of the mixing model depends on the differences in isotopic signatures between the trajectory clusters (Fig. 7) and groups (Fig. 8). This separation was less clear in MAM (Fig. 8) when precipitation maximum is observed increasing uncertainty in this season. Secondly, ~~s~~while the trajectory method determines provenance of the air masses, it does not account for moisture uptake along the transportation routes. However, our results were consistent with Wang et al. (2017) who used back trajectories adjusted using specific humidity and showed that the terrestrial moisture evaporated from Europe and CA may be the main source of precipitation in the Chinese Tien Shan. The results were also consistent with the outcomes of the moisture-tracking models. Tuinenburg et al. (2020) showed that evaporation recycling (defined as the fraction of evaporation that precipitates in the same river basin it is evaporated from) reaches 30-40% over the Tien Shan and its foothills. The annual mean of the distance which evaporated moisture travelled in a longitudinal direction is about 2-6° (Tuinenburg et al., 2020) which is consistent with the length of the local trajectories (Table 2). ~~In the future,~~ Application of a specific humidity-based model (e.g., Oza et al., 2022; ~~Oza et al., 2022, Natali et al., 2023~~) ~~(~~Natali et al., 2023~~; Oza et al., 2022~~) would be a useful follow-on study ~~may be used~~ to account for the history of moisture dynamics along the trajectories.

The third limitation was the discrepancy between the number of the identified trajectory clusters and the number of components in the mixing model imposed by the use of two tracers. To overcome this ~~problem~~, Clusters 1, 2 and 3 were merged to form Group 1 'Westerly'. This problem did not affect the CKS and CHK catchments where Group 1 was represented by a single cluster (Fig. S2). In AA clusters were merged to form Group 1 in MAM (Clusters 1 and 2 had six and two members, respectively) and SON (Clusters 1 and 2 had one and seven members, respectively). Five clusters were represented in the UA catchment only. However, there was clear seasonality in cluster occurrence at this site. The trajectory of a single precipitation event was assigned to Cluster 1 in DJF and there was no statistically significant difference between Clusters 2 and 3 ($p=0.29$) forming Group 1. By contrast, the difference between Groups 1, 2 and 3 was significant at 93% confidence level for $\delta^{18}O$ (Fig. S2). In JJA, Group 1 included 61 events assigned to Cluster 1. The different between Clusters 2 and 3 for $\delta^{18}O$ was statistically significant ($p=0.03$) but a small number of events (3 and 6, respectively) was assigned to these clusters. The difference with Cluster 1 was significant at 91% confidence level. In SON, Cluster 1 included 18 events and the difference with Clusters 2 ($n=2$) and 3 ($n=5$) was not statistically significant ($p=0.13$). Therefore, the uncertainty imposed by the limitation of the methodology is moderated by the seasonality of clusters at the UA catchment because a single cluster dominates in Group 1

Formatted: Font colour: Auto

Formatted: Font colour: Auto

in each season. In the future, this problem will be overcome by using electric conductivity of precipitation as an additional tracer in the mixing model.

~~The westerly group made the largest contribution in UA in JJA (49%) and DJF (54%), in AA in all seasons except SON (46-50%), and in CHK in JJA (73% of what is a very low precipitation total; Fig. 1).~~

~~To quantify the relative contributions of source regions to precipitation, we attempted a new approach combining the use of back trajectories with two- and three-component mixing models. One of the challenges of this approach was to reconcile the optimal number of trajectory clusters (five) with the mixing model which had a maximum of three components. We, therefore, combined three trajectory groups associated with depressions originating over the Atlantic and long-distance transport in a single group. Although Cgroups 1 (north) and 3 (Middle East) have different isotopic signatures, they, as shown above, dominated in different seasons. Small number of samples in a season or samples corresponding to some of the trajectory groups at individual sites contributed to uncertainty. For example, there were only seven samples in CKS in winter and results for this catchments and season should be treated with caution. A wide range of isotopic signatures in SON resulted in large standard errors of the mixing model in this season especially in UA (Table 3).~~

The identified significant contribution of the local sources and the extensively irrigated lower reaches of the Amu Darya and Syr Darya as well as over 80 artificial reservoirs located in this region (Xenarios et al., 2019) to precipitation in the Tien Shan poses questions about the effects of both climate change including the observed and projected increase in evaporation (Ren et al., 2022; Tuinenburg et al., 2020) and water management (Wei et al., 2013) on moisture cycling in CA. Regional evapotranspiration was previously shown to provide a significant input in precipitation especially during dry periods in the arid and semi-arid regions globally (Miralles et al., 2016). ~~The mixing model results (Table 3; Fig. 8) showed that inland recycled moisture, originating from both the vast irrigated land in the Aral Sea region and from the study catchments, is the predominant source of precipitation in the study area. Precipitation maximum in all catchments occurs in MAM except UA where it peaks in May-July (Fig. 1). In this season, precipitation associated with the local trajectories accounted for 52-54% in CKS and AA increasing to 69% in CHK. The Aral Sea region contributed 46% and 37% in UA and CKS, respectively (Table 3). In UA, 30% and 22% of precipitation in JJA were associated with trajectories originating over the Aral region. The westerly group made the largest contribution in UA in JJA (49%) and DJF (54%), in AA in all seasons except SON (46-50%), and in CHK in JJA (73% of what is a very low precipitation total; Fig. 1).~~

~~These results are consistent with Wang et al. (2017) who used back trajectories adjusted using specific humidity to show that the terrestrial moisture evaporated from Europe and CA may be the main source of precipitation in the Chinese Tien Shan. The results are also consistent with the outcomes of the moisture tracking modelling studies. Tuinenburg et al. (2020) showed that evaporation recycling (defined as the fraction of evaporation that precipitates in the same river basin it is evaporated from) reaches 30-40% over the Tien Shan and its foothills. The annual mean of the distance which evaporated moisture travelled in a longitudinal direction is about 2-6° (Tuinenburg et al., 2020) which is consistent with local trajectories (Table 2). Link et al. (2020) assessed the fraction of precipitation that originated as evaporation from terrestrial sources and showed that, in Kyrgyzstan, it reaches 61% making it one of the top 10 countries with the highest contributions from local, terrestrial sources.~~

~~We have identified a significant contribution of the local sources and the extensively irrigated lower reaches of the Amu Darya and Syr Darya as well as over 80 artificial reservoirs located in this region (Xenarios et al., 2019) to precipitation in the Tien Shan. These poses questions about the effects of both climate change including the observed and projected increase in evaporation (Ren et al., 2022; Tuinenburg et al., 2020) and water management (Wei et al., 2013) on moisture cycling in CA. Regional evapotranspiration was previously shown to provide a significant input in precipitation especially during dry periods in the arid and semi-arid regions globally (Miralles et al., 2016).~~ Water evaporated from the irrigated land contributes to precipitation over the glacierized UA and CKS catchments (and possibly CHK) contributing to snow accumulation at high

elevations in MAM which is the main accumulation season in the region. This, in turn, sustains seasonal snowpack and glaciers providing water for irrigation. A modelling study by de Kok et al. (2018) suggested that increased irrigation in the Tarim basin altered precipitation regime in a way that favoured glacier growth in the Kunlun Shan providing partial explanation to the formation of the Karakorum-Kunlun-east Pamir anomaly (Farinotti et al., 2020). Our analysis of isotopic composition of precipitation shows that the same mechanism may operate in some regions of the Tien Shan.

5 Conclusions

An important achievement of this study is the development of an extensive database of precipitation~~isotopic~~ ratios ~~of precipitation~~ and *d-excess* for the mountains of CA. These data ~~which~~have enabled analysis of geographical, ~~altitudinal~~elevational, and temporal patterns in precipitation isotopic composition, ~~of precipitation~~ and the attribution of precipitation to regional sources. ~~To date, very few measurements were available outside the Chinese sector of the Tien Shan.~~ Contributing these data to GNIP ~~(IAEA/WMO, 2015)~~ will improve the representation of the CA mountains in the global high-resolution precipitation isoscapes database~~s (Bowen and Revenaugh, 2003; Bowen et al., 2019; Terzer-Wassmuth et al., 2021)~~, especially in the cold season when the differences between modelled ~~(Bowen, 2022)~~ and measured ratios were highest ~~(Fig. 2)~~. The advantages of the developed dataset are: (i) a wide geographical coverage from the northern Tien Shan ~~(UA catchment)~~ to the Gissar-Alay foothills ~~(Dushanbe) (Fig. 1)~~; (ii) sampling at different elevations within two catchments because of the limited availability of such data globally ~~(Pang et al., 2011; Natali et al, 2022)~~; and (iii) availability of the event-based precipitation samples. ~~enabling quantification of source region contributions to CA precipitation.~~

~~The sampling programme conducted in 2019 – 2021 in the Tien Shan and its foothills produced an extensive database of isotopic ratios and D-*excess* filling a gap in isoscapes in the region where water cycle is highly sensitive to climate change.~~ The legacy of the programme is the installation of the Palmex Rain Samplers for the long-term collection of monthly precipitation samples for isotopic analysis in three catchments (Kishi Almaty, CKS, and CHK) including samplers at two elevations (700 m and 3438 m a.s.l. and away from the lake in the neighbour catchment of UA) in the Kishi Almaty catchment which will support further investigation in elevational gradients in isotopic ratios and *d*~~D~~-*excess*.

Clear annual cycles in $\delta^{18}O$ and δD ~~have been~~were identified with maxima in summer and minima in winter at all sites, while annual *d-excess* cycles highlighted the effects of local conditions on ~~the~~precipitation formation ~~of precipitation~~. Both $\delta^{18}O$ and δD values increase from north to south. These temporal and spatial patterns ~~as well as~~and the regression between air temperature and isotopic ratios showed that local air temperature controls the isotopic composition of precipitation. The relationships between $\delta^{18}O$ and δD and geographical variables ~~have been~~were quantified, ~~but~~though further investigation including a combined data set from CA and the Chinese Tien Shan ~~are~~will likely ~~generate more~~enhance result robustness ~~robust results~~.

~~The~~ LMWLs were developed for the whole region ~~as a whole~~ and for ~~the~~ individual catchments and seasons. The use of the weighted precipitation and the PWLSR method to derive LMWLs is recommended in ~~the warm season~~ JJA especially in the southern part of the region, while unweighted precipitation can be used in ~~the cold~~ other seasons and ~~in the outer ranges of~~ in the northern Tien Shan using OLSR and RMA methods ~~to derive LMWWLs~~.

For the first time, the isotopologue data were used together with back trajectories to determine the contribution of different trajectory sources to precipitation. It was shown that the combined contribution of ~~the~~ inland re-evaporated moisture from the irrigated land in the Aral basin and local moisture recycling exceeded the contribution of the longer-distance transport associated with the westerlies. ~~The back trajectory analysis enabled the identification of the main source regions of moisture~~

Formatted: Normal, Justified,Line spacing: 1.5 lines

Formatted: Font:Italic

Formatted: Font:Italic

~~which include distant (the Black and Caspian Seas region, Iran, and northern Kazakhstan - Siberia), regional (lower reaches of the Amu-Darya and Syr-Darya rivers) and local (study catchments) sources.~~ The model has several limitations and ~~For the first time, we applied a mixing model to quantify contributions of these sources to precipitation. Although the model will benefit from~~ the following improvements will be needed to confirm the initial findings: a longer sampling period enabling better separation between trajectory clusters, accounting for the history of moisture uptake along the transportation routes, and the application of additional tracers to increase the number of end members in the mixing model. However, the identified contribution of re-evaporated moisture to regional precipitation ~~its results were consistent with those of the moisture tracking models. An important finding was that a combined contribution of the inland re-evaporated moisture from the irrigated land in the Aral basin and local moisture recycling exceeded the contribution of the longer-distance transport associated with westerly depressions. This finding~~ highlights strong water loss and inefficient water management in ~~the region~~CA. It also suggests that irrigation sustained by snow and glacier melt and associated increase in evapotranspiration may benefit glacier mass balance, an issue which ~~will~~ requires further investigation. Further work to improve the spatial density of sampling sites and increase the number of samples, especially in~~s~~ the inner Tien Shan and the Pamir, is also needed to ~~help~~ confirm the findings.

Formatted: Font:10 pt, English(United Kingdom)

Formatted: Font:10 pt

Formatted: Font:10 pt, English(United Kingdom)

Acknowledgements

This work was supported by the UK Global Challenges Research Fund (GCRF). Project *'Central Asia Research and Adaptation Water Network (CARAWAN)'* supported the sampling programme across the region. Project *'Solutions for Clean Water in Central Asia: What Happens After the Ice? (SCWAI)'* supported sample processing and analysis. The sampling programme in Kazakhstan was additionally supported by the Science Committee of the Ministry of Science and Higher Education of the Republic of Kazakhstan (Grant No. BR18574176). Zarina Saidaliyeva was supported by the University of Reading International PhD Studentship. The authors are grateful to the anonymous referees for their most helpful comments.

Authors' contributions

MS, ZS, AW, and VY conceptualised the study; ZS processed samples and analysed the data, MS and AW supervised; ZS and MS wrote the original manuscript. Other authors participated in the sampling programme and provided meteorological data. All authors contributed to the discussion of results and the final version of the manuscript.

References

Aemisegger, F., Pfahl, S., Sodemann, H., Lehner, I., Seneviratne, S. I., and Wernli, H.: Deuterium excess as a proxy for continental moisture recycling and plant transpiration, Atmos. Chem. Phys., 14, 4029–4054, https://doi.org/10.5194/acp-14-4029-2014, 2014.

Aggarwal, P. K., Romatschke, U., Araguas-Araguas, L., Belachew, D., Longstaffe, F. J., Berg, P., Schumacher, C., and Funk, A.: Proportions of convective and stratiform precipitation revealed in water isotope ratios, Nat. Geosci., 9, 624–629, https://doi.org/10.1038/ngeo2739, 2016.

Aizen, E. M., Aizen, V. B., Mayewski, P. A., Zhou, H., Rodda, C., Joswiak, D., Takeuchi, N., Fujita, K., Kurbatov, A., and Grigholm, B. O.: Aridity of Central Asia through the Holocene, 2017, GC41G-02, 2017.

Aizen, V., Aizen, E., Melack, J., and Martma, T.: Isotopic measurements of precipitation on central Asian glaciers

Formatted: English(United Kingdom), Check spelling and grammar

(southeastern Tibet, northern Himalayas, central Tien Shan), J. Geophys. Res. Atmos., 101, 9185–9196, https://doi.org/10.1029/96JD00061, 1996.

Aizen, V. B., Aizen, E. M., and Melack, J. M.: Snow distribution and melt in central Tien Shan, susamir valley, Arct. Alp. Res., 29, 403–413, https://doi.org/10.2307/1551988, 1997.

Aizen, V. B., Aizen, E. M., Melack, J. M., Kreutz, K. J., and Cecil, L. D. W.: Association between atmospheric circulation patterns and firn-ice core records from the Inilchek glacierized area, central Tien Shan, Asia, J. Geophys. Res. D Atmos., 109, https://doi.org/10.1029/2003JD003894, 2004.

Aizen, V. B., Mayewski, P. A., Aizen, E. M., Joswiak, D. R., Surazakov, A. B., Kaspari, S., Grigholm, B., Krachler, M., Handley, M., and Finaev, A.: Stable-isotope and trace element time series from Fedchenko glacier (Pamirs) snow/firn cores, J. Glaciol., 55, 275–291, https://doi.org/10.3189/002214309788608787, 2009.

Araguás-Araguás, L., Froehlich, K., and Rozanski, K.: Deuterium and oxygen-18 isotope composition of precipitation and atmospheric moisture, Hydrol. Process., 14, 1341–1355, https://doi.org/10.1002/1099-1085(20000615)14:8<1341::AID-HYP983>3.3.CO;2-Q, 2000.

Bagheri, R., Bagheri, F., Karami, G. H., and Jafari, H.: Chemo-isotopes (18O & 2H) signatures and HYSPLIT model application: Clues to the atmospheric moisture and air mass origins, Atmos. Environ., 215, 116892, https://doi.org/10.1016/j.atmosenv.2019.116892, 2019.

Bershaw, J.: Controls on deuterium excess across Asia, Geosci., 8, https://doi.org/10.3390/geosciences8070257, 2018.

Bowen, G. J.: Isoscapes: Spatial Pattern in Isotopic Biogeochemistry, Annu. Rev. Earth Planet. Sci., 38, 161–187, https://doi.org/10.1146/annurev-earth-040809-152429, 2010.

Bowen, G. J.: The Online Isotopes in Precipitation Calculator, version OIPC3.1. http://www.waterisotopes.org, 2022.

Bowen, G. J., Kennedy, C. D., Henne, P. D., and Zhang, T.: Footprint of recycled water subsidies downwind of Lake Michigan, 3, art53, https://doi.org/10.1890/ES12-00062.1, 2012.

Bowen, G. J., Putman, A., Brooks, J. R., Bowling, D. R., Oerter, E. J., and Good, S. P.: Inferring the source of evaporated waters using stable H and O isotopes, Oecologia, 187, 1025–1039, https://doi.org/10.1007/s00442-018-4192-5, 2018.

Bowen, G. J., Cai, Z., Fiorella, R. P., and Putman, A. L.: Isotopes in the Water Cycle: Regional- to Global-Scale Patterns and Applications, Annu. Rev. Earth Planet. Sci., 47, 453–479, https://doi.org/10.1146/annurev-earth-053018-060220, 2019.

Chen, F., Wang, S., Wu, X., Zhang, M., Argiriou, A. A., Zhou, X., and Chen, J.: Local Meteoric Water Lines in a Semi-Arid Setting of Northwest China Using Multiple Methods, 13, 2380, https://doi.org/10.3390/w13172380, 2021.

Chen, L., Zhu, G., Lin, X., Li, R., Lu, S., Jiao, Y., Qiu, D., Meng, G., and Wang, Q.: The Complexity of Moisture Sources Affects the Altitude Effect of Stable Isotopes of Precipitation in Inland Mountainous Regions, Water Resour. Res., 60, https://doi.org/10.1029/2023WR036084, 2024.

Consortium, R.: Randolph glacier inventory–a dataset of global glacier outlines: Version 6.0: technical report, global land ice measurements from space, Colorado, USA, Digit. Media. https//doi. org/10.7265, 2017.

Craig, H.: Isotopic Variations in Meteoric Waters, Science (80-.)., 133, 1702–1703, https://doi.org/10.1126/science.133.3465.1702, 1961.

Craig, H. and Gordon, L.: Deuterium and oxygen 18 variations in the ocean and the marine atmosphere, 9–130 pp., 1965.

Crawford, J., Hughes, C. E., and Lykoudis, S.: Alternative least squares methods for determining the meteoric water line, demonstrated using GNIP data, J. Hydrol., 519, 2331–2340, https://doi.org/10.1016/j.jhydrol.2014.10.033, 2014.

Dansgaard, W.: Stable isotopes in precipitation, Tellus A Dyn. Meteorol. Oceanogr., 16, 436, https://doi.org/10.3402/tellusa.v16i4.8993, 1964.

Dorling, S. R., Davies, T. D., and Pierce, C. E.: Cluster analysis : a technique for estimating the synoptic meteorological controls on air and precipitation chemistry--results from Eskdalemuir, South Scotland, Atmos. Environ., 26, 2583–2602, 1992.

Draxler, R. R. and Rolph, G. D.: HYSPLIT (HYbrid Single-Particle Lagrangian Integrated Trajectory) Model access via NOAA ARL READY Website, NOAA Air Resour. Lab. Silver Spring, MD, http://ready.arl.noaa.gov/HYSPLIT.php, 2013.

Van Der Ent, R. J. and Tuinenburg, O. A.: The residence time of water in the atmosphere revisited, Hydrol. Earth Syst. Sci., 21, 779–790, https://doi.org/10.5194/hess-21-779-2017, 2017.

Farinotti, D., Longuevergne, L., Moholdt, G., Duethmann, D., Mölg, T., Bolch, T., Vorogushyn, S., and Güntner, A.: Substantial glacier mass loss in the Tien Shan over the past 50 years, Nat. Geosci., 8, 716–722, https://doi.org/10.1038/ngeo2513, 2015.

Farinotti, D., Immerzeel, W. W., de Kok, R. J., Quincey, D. J., and Dehecq, A.: Manifestations and mechanisms of the Karakoram glacier Anomaly, Nat. Geosci., 13, 8–16, https://doi.org/10.1038/s41561-019-0513-5, 2020.

Friedman, I., Machta, L., and Soller, R.: Water-vapor exchange between a water droplet and its environment, J. Geophys. Res., 67, 2761–2766, https://doi.org/10.1029/JZ067i007p02761, 1962.

Froehlich, K., Kralik, M., Papesch, W., Rank, D., Scheifinger, H., and Stichler, W.: Deuterium excess in precipitation of Alpine regions – moisture recycling, Isotopes Environ. Health Stud., 44, 61–70, https://doi.org/10.1080/10256010801887208, 2008.

Gat, J. R.: Oxygen and Hydrogen Isotopes in the Hydrologic Cycle, Annu. Rev. Earth Planet. Sci., 24, 225–262, https://doi.org/10.1146/annurev.earth.24.1.225, 1996.

Gat, J. R. and Gonfiantini, R.: Stable Isotope Hydrology Deuterium and Oxygen-18 in the Water Cycle. Inte, rnational At. energy agency, 339, 1981.

He, Z., Unger-shayesteh, K., Vorogushyn, S., Weise, S. M., Kalashnikova, O., Gafurov, A., Duethmann, D., Barandun, M., and Merz, B.: Constraining hydrological model parameters using water isotopic compositions in a glacierized basin , Central Asia, 571, 332–348, https://doi.org/10.1016/j.jhydrol.2019.01.048, 2019.

Hoelzle, M., Barandun, M., Bolch, T., Fiddes, J., Gafurov, A., Muccione, V., Saks, T., and Shahgedanova, M.: The status and role of the alpine cryosphere in Central Asia, Aral Sea Basin Water Sustain. Dev. Cent. Asia, 2, 100–121, https://doi.org/10.4324/9780429436475-8, 2019.

Hughes, C. E. and Crawford, J.: A new precipitation weighted method for determining the meteoric water line for hydrological applications demonstrated using Australian and global GNIP data, J. Hydrol., 464–465, 344–351, https://doi.org/10.1016/j.jhydrol.2012.07.029, 2012.

IAEA/WMO: Global Network of Isotopes in Precipitation. The GNIP Database. Accessible at: https://nucleus.iaea.org/wiser., 2015.

Formatted: English(United Kingdom)

Immerzeel, W. W., Lutz, A. F., Andrade, M., Bahl, A., Biemans, H., Bolch, T., Hyde, S., Brumby, S., Davies, B. J., Elmore, A. C., Emmer, A., Feng, M., Fernández, A., Haritashya, U., Kargel, J. S., Koppes, M., Kraaijenbrink, P. D. A., Kulkarni, A. V., Mayewski, P. A., Nepal, S., Pacheco, P., Painter, T. H., Pellicciotti, F., Rajaram, H., Rupper, S., Sinisalo, A., Shrestha, A. B., Viviroli, D., Wada, Y., Xiao, C., Yao, T., and Baillie, J. E. M.: Importance and vulnerability of the world's water towers, Nature, 577, 364–369, https://doi.org/10.1038/s41586-019-1822-y, 2020.

Jasechko, S.: Global Isotope Hydrogeology—Review, Rev. Geophys., 57, 835–965, https://doi.org/10.1029/2018RG000627, 2019.

Jiang, J., Zhou, T., Chen, X., and Zhang, L.: Future changes in precipitation over Central Asia based on CMIP6 projections, Environ. Res. Lett., 15, https://doi.org/10.1088/1748-9326/ab7d03, 2020.

Jin, L., Chen, F., Morrill, C., Otto-Bliesner, B. L., and Rosenbloom, N.: Causes of early Holocene desertification in arid central Asia, Clim. Dyn., 38, 1577–1591, https://doi.org/10.1007/s00382-011-1086-1, 2012.

Jorba, O., Pérez, C., Rocadenbosch, F., and Baldasano, J.: Cluster Analysis of 4-Day Back Trajectories Arriving in the Barcelona Area, Spain, from 1997 to 2002, J. Appl. Meteorol., 43, 887–901, https://doi.org/10.1175/1520-0450(2004)043<0887:CAODBT>2.0.CO;2, 2004.

Juhlke, T. R., Meier, C., Van Geldern, R., Vanselow, K. A., Wernicke, J., Baidulloeva, J., Barth, J. A. C., and Weise, S. M.: Assessing moisture sources of precipitation in the Western Pamir Mountains (Tajikistan, Central Asia) using deuterium excess, Tellus B Chem. Phys. Meteorol., 71, 1601987, https://doi.org/10.1080/16000889.2019.1601987, 2019.

Kapitsa, V., Shahgedanova, M., Severskiy, I., Kasatkin, N., White, K., and Usmanova, Z.: Assessment of Changes in Mass Balance of the Tuyuksu Group of Glaciers, Northern Tien Shan, Between 1958 and 2016 Using Ground-Based Observations and Pléiades Satellite Imagery, Front. Earth Sci., 8, https://doi.org/10.3389/feart.2020.00259, 2020.

Kaser, G., Großhauser, M., and Marzeion, B.: Contribution potential of glaciers to water availability in different climate regimes, Proc. Natl. Acad. Sci. U. S. A., 107, 20223–20227, https://doi.org/10.1073/pnas.1008162107, 2010.

de Kok, R. J., Tuinenburg, O. A., Bonekamp, P. N. J., and Immerzeel, W. W.: Irrigation as a Potential Driver for Anomalous Glacier Behavior in High Mountain Asia, Geophys. Res. Lett., 45, 2047–2054, https://doi.org/10.1002/2017GL076158, 2018.

Kostrova, S. S., Meyer, H., Fernandoy, F., Werner, M., and Tarasov, P. E.: Moisture origin and stable isotope characteristics of precipitation in southeast Siberia, Hydrol. Process., 34, 51–67, https://doi.org/10.1002/hyp.13571, 2020.

Kreutz, K. J., Wake, C. P., Aizen, V. B., DeWayne Cecil, L., and Synal, H. A.: Seasonal deuterium excess in a Tien Shan ice core: Influence of moisture transport and recycling in Central Asia, Geophys. Res. Lett., 30, https://doi.org/10.1029/2003GL017896, 2003.

Kutuzov, S. and Shahgedanova, M.: Glacier retreat and climatic variability in the eastern Terskey-Alatoo, inner Tien Shan between the middle of the 19th century and beginning of the 21st century, Glob. Planet. Change, 69, 59–70, https://doi.org/10.1016/j.gloplacha.2009.07.001, 2009.

Lachniet, M. S. and Patterson, W. P.: Use of correlation and stepwise regression to evaluate physical controls on the stable isotope values of Panamanian rain and surface waters, J. Hydrol., 324, 115–140, https://doi.org/10.1016/j.jhydrol.2005.09.018, 2006.

Liu, J., Song, X., Yuan, G., Sun, X., and Yang, L.: Stable isotopic compositions of precipitation in China, Tellus B Chem.

Phys. Meteorol., 66, 22567, https://doi.org/10.3402/tellusb.v66.22567, 2014.

Lydolph, P. E.: Climates of the Soviet Union, edited by: Paul E. Lydolph and Landsberg, H. E., Elsevier Scientific Publishing Company, 443 pp., 1977.

Minder, J. R., Bartolini, W. M., Spence, C., Hedstrom, N. R., Blanken, P. D., and Lenters, J. D.: Characterizing and constraining uncertainty associated with surface and boundary layer turbulent fluxes in simulations of lake-effect snowfall, Weather Forecast., 35, 467–488, https://doi.org/10.1175/WAF-D-19-0153.1, 2020.

Miralles, D. G., Nieto, R., McDowell, N. G., Dorigo, W. A., Verhoest, N. E. C., Liu, Y. Y., Teuling, A. J., Dolman, A. J., Good, S. P., and Gimeno, L.: Contribution of water-limited ecoregions to their own supply of rainfall, Environ. Res. Lett., 11, https://doi.org/10.1088/1748-9326/11/12/124007, 2016.

Natali, S., Doveri, M., Giannecchini, R., Baneschi, I., and Zanchetta, G.: Is the deuterium excess in precipitation a reliable tracer of moisture sources and water resources fate in the western Mediterranean? New insights from Apuan Alps (Italy), J. Hydrol., 614, https://doi.org/10.1016/j.jhydrol.2022.128497, 2022.

Natali, S., Doveri, M., Franceschi, L., Giannecchini, R., Luppichini, M., Menichini, M., and Zanchetta, G.: Moisture sources and climatic effects controlling precipitation stable isotope composition in a western Mediterranean island (Pianosa, Italy), Atmos. Res., 294, 106987, https://doi.org/10.1016/j.atmosres.2023.106987, 2023.

Oza, H., Padhya, V., Ganguly, A., and Deshpande, R. D.: Investigating hydrometeorology of the Western Himalayas: Insights from stable isotopes of water and meteorological parameters, Atmos. Res., 268, 105997, https://doi.org/10.1016/j.atmosres.2021.105997, 2022.

Pang, Z., Kong, Y., Froehlich, K., Huang, T., Yuan, L., Li, Z., and Wang, F.: Processes affecting isotopes in precipitation of an arid region, Tellus B Chem. Phys. Meteorol., 63, 352, https://doi.org/10.1111/j.1600-0889.2011.00532.x, 2011.

Pérez, I. A., Artuso, F., Mahmud, M., Kulshrestha, U., Sánchez, M. L., and García, M. Á.: Applications of Air Mass Trajectories, Adv. Meteorol., 2015, 1–20, https://doi.org/10.1155/2015/284213, 2015.

Phillips, D. L. and Gregg, J. W.: Uncertainty in source partitioning using stable isotopes, Oecologia, 127, 171–179, https://doi.org/10.1007/s004420000578, 2001.

Putman, A. L., Fiorella, R. P., Bowen, G. J., and Cai, Z.: A Global Perspective on Local Meteoric Water Lines: Meta-analytic Insight Into Fundamental Controls and Practical Constraints, Water Resour. Res., 55, 6896–6910, https://doi.org/10.1029/2019WR025181, 2019.

Ren, Y., Yu, H., Liu, C., He, Y., Huang, J., Zhang, L., Hu, H., Zhang, Q., Chen, S., Liu, X., Zhang, M., Wei, Y., Yan, Y., Fan, W., and Zhou, J.: Attribution of Dry and Wet Climatic Changes over Central Asia, J. Clim., 35, 1399–1421, https://doi.org/10.1175/JCLI-D-21-0329.1, 2022.

Rolph, G., Stein, A., and Stunder, B.: Real-time Environmental Applications and Display sYstem: READY, Environ. Model. Softw., 95, 210–228, https://doi.org/10.1016/j.envsoft.2017.06.025, 2017.

Rozanski, K., Araguás-Araguás, L., and Gonfiantini, R.: Isotopic Patterns in Modern Global Precipitation, in: Journal of Geophysical Research Atmospheres, 1–36, https://doi.org/10.1029/GM078p0001, 2013.

Severskiy, I., Vilesov, E., Armstrong, R., Kokarev, A., Kogutenko, L., Usmanova, Z., Morozova, V., and Raup, B.: Changes in glaciation of the Balkhash–Alakol basin, central Asia, over recent decades, Ann. Glaciol., 57, 382–394, https://doi.org/10.3189/2016AoG71A575, 2016.

Shahgedanova, M.: In: The Physical Geography of Northern Eurasia: Russia and Neighbouring States., in: Climate at Present and in the Historical Past., Oxford University Press, 70–102, 2002.

Shahgedanova, M., Afzal, M., Severskiy, I., Usmanova, Z., Saidaliyeva, Z., Kapitsa, V., Kasatkin, N., and Dolgikh, S.: Changes in the mountain river discharge in the northern Tien Shan since the mid-20th Century: Results from the analysis of a homogeneous daily streamflow data set from seven catchments, J. Hydrol., 564, 1133–1152, https://doi.org/10.1016/j.jhydrol.2018.08.001, 2018.

Stein, A. F., Draxler, R. R., Rolph, G. D., StundeR, B. J. B., Cohen, M. D., and Ngan, F.: Noaa's hysplit atmospheric transport and dispersion modeling system, Bull. Amer. Meteor. Soc., 96, 2059–2078, https://doi.org/https://doi.org/10.1175/BAMS-D-14-00110.1, 2015.

Tian, L., Yao, T., MacClune, K., White, J. W. C., Schilla, A., Vaughn, B., Vachon, R., and Ichiyanagi, K.: Stable isotopic variations in west China: A consideration of moisture sources, J. Geophys. Res. Atmos., 112, 1–12, https://doi.org/10.1029/2006JD007718, 2007.

Tuinenburg, O. A., Theeuwen, J. J. E., and Staal, A.: High-resolution global atmospheric moisture connections from evaporation to precipitation, Earth Syst. Sci. Data, 12, 3177–3188, https://doi.org/10.5194/essd-12-3177-2020, 2020.

Viviroli, D., Kummu, M., Meybeck, M., Kallio, M., and Wada, Y.: Increasing dependence of lowland populations on mountain water resources, Nat. Sustain., https://doi.org/10.1038/s41893-020-0559-9, 2020.

Wang, L., Dong, Y., Han, D., and Xu, Z.: Stable isotopic compositions in precipitation over wet island in Central Asia, J. Hydrol., 573, 581–591, https://doi.org/10.1016/j.jhydrol.2019.04.005, 2019.

Wang, S., Zhang, M., Che, Y., Chen, F., and Qiang, F.: Contribution of recycled moisture to precipitation in oases of arid central Asia: A stable isotope approach, Water Resour. Res., 52, 3246–3257, https://doi.org/10.1002/2015WR018135, 2016a.

Wang, S., Zhang, M., Hughes, C. E., Zhu, X., Dong, L., Ren, Z., and Chen, F.: Factors controlling stable isotope composition of precipitation in arid conditions: an observation network in the Tianshan Mountains, central Asia, Tellus B Chem. Phys. Meteorol., 68, 26206, https://doi.org/10.3402/tellusb.v68.26206, 2016b.

Wang, S., Zhang, M., Crawford, J., Hughes, C. E., Du, M., and Liu, X.: The effect of moisture source and synoptic conditions on precipitation isotopes in arid central Asia, J. Geophys. Res. Atmos., 122, 2667–2682, https://doi.org/10.1002/2015JD024626, 2017.

Wang, S., Zhang, M., Hughes, C. E., Crawford, J., Wang, G., Chen, F., Du, M., Qiu, X., and Zhou, S.: Meteoric water lines in arid Central Asia using event-based and monthly data, J. Hydrol., 562, 435–445, https://doi.org/10.1016/j.jhydrol.2018.05.034, 2018.

Wang, S., Wang, L., Zhang, M., Shi, Y., Hughes, C. E., Crawford, J., Zhou, J., and Qu, D.: Quantifying moisture recycling of a leeward oasis in arid central Asia using a Bayesian isotopic mixing model, J. Hydrol., 613, 128459, https://doi.org/10.1016/j.jhydrol.2022.128459, 2022.

Wassenaar, L., Terzer-Wassmuth, S., and Douence, C.: Progress and challenges in dual- and triple-isotope ($\delta^{18}O$, $\delta^{2}H$, $\Delta^{17}O$) analyses of environmental waters: An international assessment of laboratory performance, Rapid Commun. Mass Spectrom., 35, 1–12, https://doi.org/10.1002/rcm.9193, 2021.

Wei, J., Dirmeyer, P. A., Wisser, D., Bosilovich, M. G., and Mocko, D. M.: Where Does the Irrigation Water Go? An

Formatted: English(United Kingdom)

Formatted: English(United Kingdom)

Formatted: English(United Kingdom)

Estimate of the Contribution of Irrigation to Precipitation Using MERRA, J. Hydrometeorol., 14, 275–289, https://doi.org/10.1175/JHM-D-12-079.1, 2013.

Wu, H., Zhang, X., Xiaoyan, L., Li, G., and Huang, Y.: Seasonal variations of deuterium and oxygen-18 isotopes and their response to moisture source for precipitation events in the subtropical monsoon region, Hydrol. Process., 29, 90–102, https://doi.org/10.1002/hyp.10132, 2015.

Xenarios, S., Schmidt-Vogt, D., Qadir, M., Janusz-Pawletta, B., and Abdullaev, I. (Eds.): The Aral Sea Basin. Water for sustainable development in Central Asia, Routledge, 227 pp., https://doi.org/10.4324/9780429436475, 2019.

Xiao, W., Lee, X., Hu, Y., Liu, S., Wang, W., Wen, X., Werner, M., and Xie, C.: An Experimental Investigation of Kinetic Fractionation of Open-Water Evaporation Over a Large Lake, J. Geophys. Res. Atmos., 122, 11,651-11,663, https://doi.org/10.1002/2017JD026774, 2017.

Yang, X., Acharya, S., and Yao, T.: Vertical Profile of Meteoric and Surface-Water Isotopes in Nepal Himalayas to Everest's Summit, Atmosphere (Basel)., 14, 202, https://doi.org/10.3390/atmos14020202, 2023.

Yapiyev, V., Skrzypek, G., Verhoef, A., Macdonald, D., and Sagintayev, Z.: Between boreal Siberia and arid Central Asia – Stable isotope hydrology and water budget of Burabay National Nature Park ecotone (Northern Kazakhstan), J. Hydrol. Reg. Stud., 27, 100644, https://doi.org/10.1016/j.ejrh.2019.100644, 2020.

Yoshimura, K.: Stable water isotopes in climatology, meteorology, and hydrology: A review, J. Meteorol. Soc. Japan, 93, 513–533, https://doi.org/10.2151/jmsj.2015-036, 2015.

Zhang, M. and Wang, S.: Precipitation isotopes in the Tianshan Mountains as a key to water cycle in arid central Asia, Sci. Cold Arid Reg., https://doi.org/10.3724/SP.J.1226.2018.00027, 2018.

Zongxing, L., Qi, F., Song, Y., Wang, Q. J., Yang, J., Yongge, L., Jianguo, L., and Xiaoyan, G.: Stable isotope composition of precipitation in the south and north slopes of Wushaoling Mountain, northwestern China, Atmos. Res., 182, 87–101, https://doi.org/10.1016/j.atmosres.2016.07.023, 2016.